AD-A039 059 UNITED TECHNOLOGIES RESEARCH CENTER EAST HARTFORD CONN F/G 13/8
EVALUATION OF BASIC LASER WELDING CAPABILITIES.(U)
MAR 77 E M BREINAN, C M BANAS, G P MCCARTHY N00014-74-C-0423
UNCLASSIFIED UTRC/R77-911989-10 NL

| OF |
AD
A039059

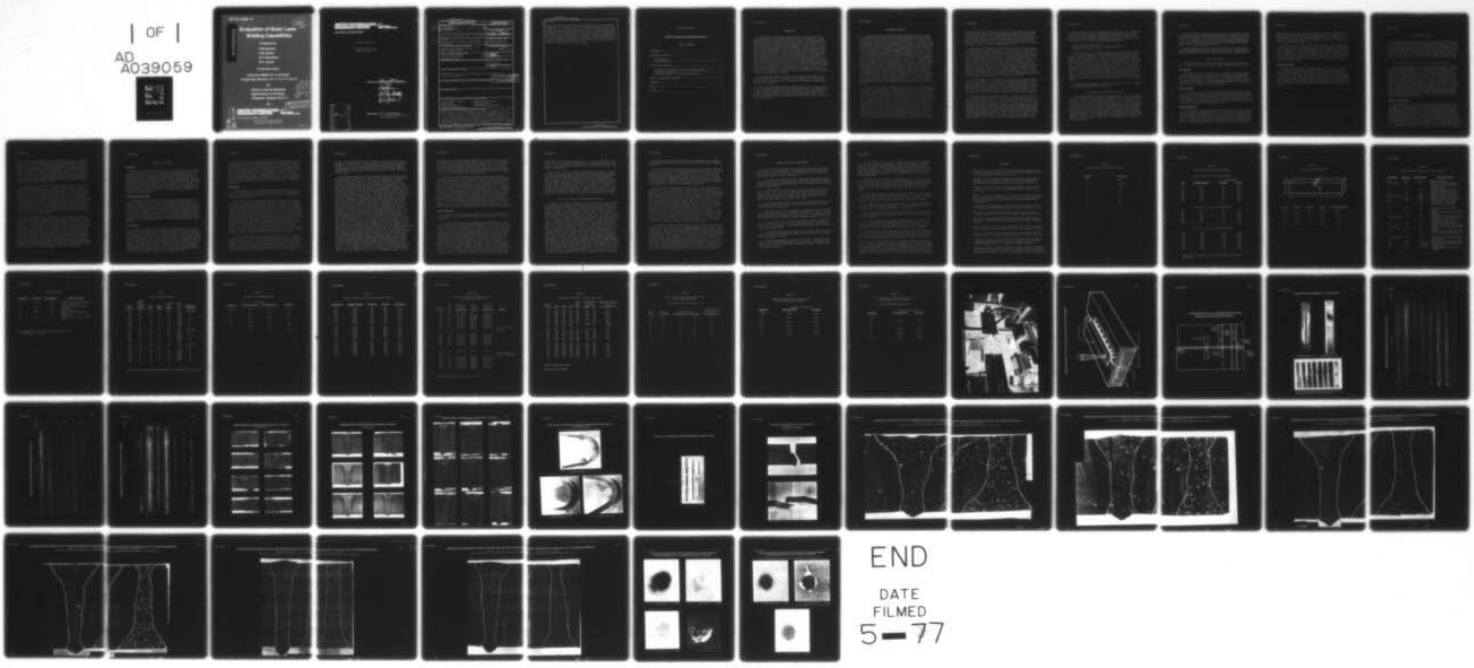

END

DATE
FILMED
5-77

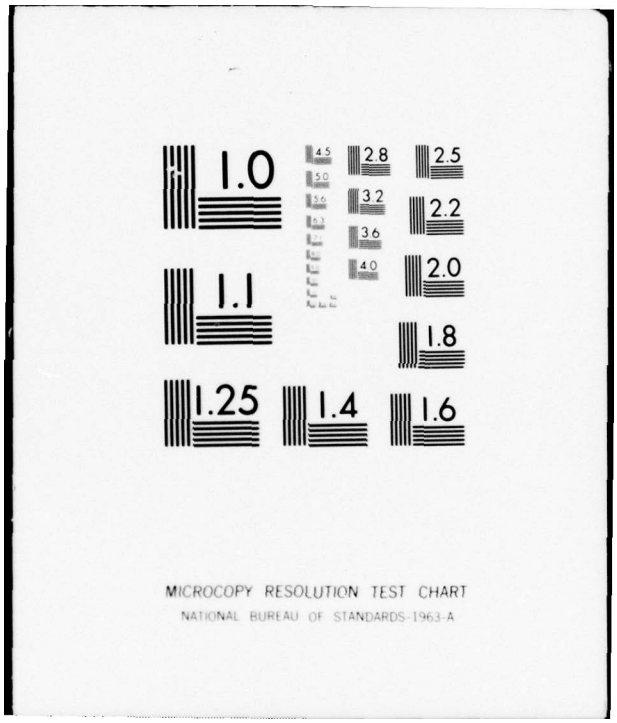
1.0
1.1
1.25
1.4
1.6
1.8
2.0
2.2
2.5
2.8
3.2
3.6
4.0
4.5
5.0
5.6
MICROCOPY RESOLUTION TEST CHART
NATIONAL BUREAU OF STANDARDS-1963-A

R77-911989-10

Evaluation of Basic Laser Welding Capabilities

Prepared by

E.M. Breinan

C.M. Banas

G.P. McCarthy

B.A. Jacob

Technical report

Contract N00014-74-C-0423

Project No. NR 031-771/1-31-77 (471)

for

Office of Naval Research

Department of the Navy

Arlington, Virginia 22217

by

UNITED TECHNOLOGIES RESEARCH CENTER

EAST HARTFORD, CONNECTICUT 06108

UNITED TECHNOLOGIES

77-02-113-1

UNITED TECHNOLOGIES RESEARCH CENTER

UNITED TECHNOLOGIES

East Hartford, Connecticut 06108

Report R77-911989-10

Evaluation of Basic Laser Welding Capabilities

REPORTED BY Edward M. Breinan
E. M. Breinan

C. M. Banas

G. P. McCarthy

B. A. Jacob

APPROVED BY F. S. Galasso
F. S. Galasso, Principal Scientist
Materials Synthesis

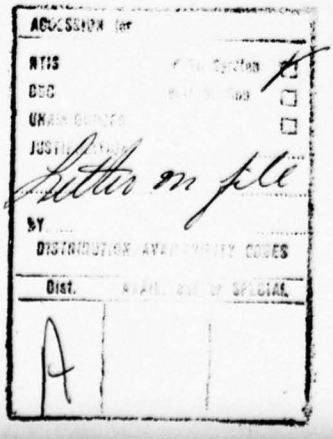

UNCLASSIFIED

SECURITY CLASSIFICATION OF THIS PAGE (When Data Entered)

REPORT DOCUMENTATION PAGE

READ INSTRUCTIONS BEFORE COMPLETING FORM

1. REPORT NUMBER: UTRC/R77-911989-10	2. GOVT ACCESSION NO.
3. RECIPIENT'S CATALOG NUMBER	
4. TITLE (and Subtitle): EVALUATION OF BASIC LASER WELDING CAPABILITIES	5. TYPE OF REPORT & PERIOD COVERED: Technical Report, Nov. 1975 - Feb. 1977
	6. PERFORMING ORG. REPORT NUMBER
7. AUTHOR(s): Edward M. Breinan, C. M. Banas, G. P. McCarthy, B. A. Jacob	8. CONTRACT OR GRANT NUMBER(s): N00014-74-C-0423
9. PERFORMING ORGANIZATION NAME AND ADDRESS: United Technologies Research Center, East Hartford, CT 06108	10. PROGRAM ELEMENT, PROJECT, TASK AREA & WORK UNIT NUMBERS: 12 59 p.
11. CONTROLLING OFFICE NAME AND ADDRESS: Office of Naval Research, Department of the Navy, Arlington, VA 22217	12. REPORT DATE: Mar. 1977
	13. NUMBER OF PAGES: 51
14. MONITORING AGENCY NAME & ADDRESS (if different from Controlling Office)	15. SECURITY CLASS. (of this report): Unclassified
	15a. DECLASSIFICATION/DOWNGRADING SCHEDULE

16. DISTRIBUTION STATEMENT (of this Report)

Reproduction in whole or in part is permitted for any purpose of the United States Government

DISTRIBUTION STATEMENT A
Approved for public release;
Distribution Unlimited

17. DISTRIBUTION STATEMENT (of the abstract entered in Block 20, if different from Report)

18. SUPPLEMENTARY NOTES

19. KEY WORDS (Continue on reverse side if necessary and identify by block number)

Laser Materials Processing
Laser Welding
Fundamental Studies
HY-130 Laser Weld Properties
Fusion Zone Purification
Dynamic Tear Tests
Laser Weld Process Feasibility

20. ABSTRACT (Continue on reverse side if necessary and identify by block number)

HY-130 alloy steel was laser-welded in a series of thicknesses including 0.64, 0.95, and 1.27 cm at continuous laser powers ranging from 6.0 to 12.8 kW and speeds between 1.27 and 2.96 cm/sec. All welds were visually inspected, X-rayed, magnafluxed, and subjected to a series of mechanical tests including hardness, bend, tensile, impact, and dynamic tear tests. Although some of the specimens, primarily those of intermediate thickness (0.95 cm),

DD FORM 1 JAN 73 1473 EDITION OF 1 NOV 65 IS OBSOLETE
S/N 0102-014-6601

UNCLASSIFIED 409 252
SECURITY CLASSIFICATION OF THIS PAGE (When Data Entered)

#20 Cont'd

encountered porosity problems during laser welding, all specimens performed extremely well in mechanical tests. Based on the sum total results, it was concluded that the laser welding process is capable of making acceptable and mechanically excellent welds in HY-130 alloy steel through 1.27 cm thickness. Weldability of the alloy was found to be improved by better deoxidation practice in the original steelmaking (i.e. rare-earth treatment), although substantial elimination of inclusions by the Fusion Zone Purification effect was observed and quantitatively verified in all cases of HY-130 laser welding encountered during the course of this study.

Report R77-911989-10

Evaluation of Basic Laser Welding Capabilities

TABLE OF CONTENTS

INTRODUCTION

Initial work in this research program has been directed toward a basic understanding of the laser welding process by means of studies of the primary mechanisms involved in deep-penetration laser welding. The fundamental information generated by this initial work is applicable to all metals and alloys having known physical properties, and was reported in detail in Ref. 1. During the continued course of laser welding development, various questions have been raised on both the fundamental and practical sides. These included two situations of high current interest to the Navy; the welding of HY-130 alloy steel and aluminum alloy welding. In HY-130 welding, as well as in deep-penetration laser welding of other alloys, excellent weld properties had been achieved apparently through purification of the fusion zone during welding (Refs. 2,3). One objective of the present work which has been accomplished and is reported in detail herein is a more precise definition of the fusion zone purification effects which take place during HY-130 laser welding. The study of this specific effect still yields information which is potentially broad in nature, since the fusion zone purification effect has already been shown to be applicable to other materials. The possibility of using this technique specifically for material purification during processing also exists.

The other area, aluminum welding, is currently under investigation and, although steady progress is being made, more work remains to be done, and, as the HY-130 work nears completion, the emphasis in the program is being shifted towards aluminum welding.

Other basic work planned included studies of the effects of welding atmosphere, gas composition and pressure on welding response and a more detailed look at laser operational parameters. Interesting effects of gas atmosphere have already been noted and will be discussed in future technical reports. These observations may eventually influence the ways in which future laser weld shielding is accomplished.

EXPERIMENTAL PROCEDURE

All welding performed during the present program was accomplished using the continuous, cross beam CO_2 laser developed under NOSC/NOL Contract N60921-70-C-0219. This laser operates as an oscillator/amplifier with output in the TEM_{00} fundamental mode and is described in detail in Ref. 4. Continuous power at outputs to at least 16.0 kW are available for welding tests using this device, as modified to its present capability. For welding, the horizontal output beam from the laser was directed upward by a plane turning mirror into a downward-facing focusing mirror to provide downhand welding conditions as shown in Fig. 1. A 18 in. (45.7 cm) focal length (f/6) spherical focusing element was used, and provided an effective minimum spot diameter of approximately 0.040 in. (0.100 cm) at the focal point. At the 10 kW power level, this spot diameter represents an incident power density of 8×10^6 W/in^2 (1.2×10^6 W/cm^2) at the workpiece surface. Although the high power weld fixture shown in Fig. 1 incorporates provisions for translating the focused beam over a stationary workpiece, the HY-130 welds made in this study were formed by moving the samples under a fixed beam with a precision x-y table incorporating a variable speed drive. Welding was accomplished in the deep penetration mode, with the power density applied to the workpiece, and the interaction time (welding speed) controlled so that a stable vapor column is created through the thickness dimension of the workpiece. Surrounding this vapor column is a liquid pool, which, when translated along a joint to be welded causes fusion of the two pieces. Relative motion between the laser and the parts being welded was achieved, in the case of this study, by translating the work using drive-screw type mechanisms powered by electric motors.

The plates to be welded were prepared with flat, square, butt-joint surfaces produced by Blanchard grinding. Following grinding, the plates were cleaned by washing in a vapor degreaser and wiped with acetone and then alcohol to remove any residues from the joint areas. A schematic diagram of the fixturing used to hold the plates to be welded is shown in Fig. 2. The base plate was fabricated from aluminum, with a generous relief groove provided under the root of the weld. A backup gas, argon, was bled into the relief groove to shield the roots, or underbead sides of the welds as they were formed. In order to shield the weld penetration cavity and puddle and the hot weld immediately following its formation from atmospheric gases, a gas shielding enclosure was carried above the weld joint. The laser beam was focused on the work through a hole in the forward end of this enclosure. The shielding gas in the area of the beam was He-20% A and was applied nearly parallel to the workpiece surface, in the direction of the weld progress. This served to blow any plasma, smoke, fumes, and other contaminants away from the shielded area. In addition, it was hoped

that by flowing the shielding gas parallel to the work, rather than impinging it normal to the work, atmosphere-borne impurities would not be driven excessively toward the weld, i.e. the momentum gradient toward the weld would be minimized, and, in fact, vaporized inclusions might even tend to be aspirated from the deep penetration cavity and carried away in this gas stream. The vaporized inclusions are involved with the fusion zone purification phenomenon under study, and are discussed in greater detail below.

To complete the shielding, a trailer shield 5 in. (12.7 cm) long was used to cover the hot, just-solidified weld as it emerged from the vicinity of the laser focal point. Argon, a heavy gas, was flowed vertically downward and to the sides within this trailer shield, which was not unlike that which has been used for Gas Tungsten Arc (GTA) welding. A photograph of the HY-130 welding setup, including fixturing of the plates to be welded, appeared in Fig. 1. It can be seen that a slight, sideways clamping force is exerted by a series of screw threads, in order to force the parts being joined solidly against one another. It is of interest to note that even though heat is added to the parts during welding and they experience some thermal expansion, clamping pressure does not increase, but rather is lost following welding. This is due to the fact that the plates shrink and draw together during welding, and, in fact, the material in the underbead (root) and overbead (face) reinforcement are produced by this drawing together (shrinkage) of the liquid in the bead.

Prior to welding, the He-Ne alignment laser was used to locate the seam at two points on opposite ends. Each point of location was marked with a laser spot weld, after which no further alignment adjustments were permitted. The spot weld thus served two purposes. By having two definite points of location along a straight linear path, the weld joint was positively located. At the same time the two spot welds served to tack weld the parts together, assuring that there would be no relative motion between them during further welding.

Three series of HY-130 welds were produced. Plates 4 in. x 8 in. (10.2 x 20.4 cm) were butt welded to form 8 in. (20.4 cm) square welded plates. The series designated A was produced in nominal quarter-inch (0.64 cm) thick plate, the B series in nominal three-eights inch (0.95 cm) plate, and the C series in one-half inch (1.27 cm) thick plate. All HY-130 plate was supplied by the Navy through the Naval Ship Research and Development Center, Annapolis, Maryland. The plate was typical of that being used in other Navy HY-130 welding research programs. Heat numbers and specific chemical analyses were not provided, however the nominal chemical analysis of HY-130 alloy is given in Table I for the major alloying elements present. During the course of this research, other specific analyses were conducted and will be discussed below under results.

The welding conditions for the three series of HY-130 welds are summarized in Table II. In each thickness, conditions were modified until the welding process was quietly and smoothly accomplished and the face and root bead profiles appeared to be acceptable. The gas-shielding conditions applied to the welds included the following flow rates and gas compositions:

relief groove area: argon: 20 cfh
beam/workpiece interaction point: helium-20% argon: 80 cfh
trailer shield: argon: 20 cfh.

Following welding, all plates were visually inspected and were classified as to the weld bead appearance. Further inspection was accomplished by radiography. Standard radiographic techniques were used in accordance with AMS Specification 2635. Exposures were for one minute using tungsten X-rays. All thicknesses were observed at 10 Ma current, 48 in. (122 cm) target to film distance using Kodak M film and with a .005 in. (.013 cm) lead screen on both the front and back of the film casette. Voltages were 180 KV for 0.64 cm thick material, 215 KV for 0.95 cm thick material, and 240 KV for 1.27 cm thick material. Stainless steel penetrometers having hole sizes of 0.010, 0.020, and 0.040 in. (0.025, 0.051, and 0.102 cm) diameter and thicknesses equal to two percent of the specimen thickness were used as a standard for resolution. All penetrometer holes were resolvable in the processed films with the 0.025 cm diameter holes being just barely discernible, and hence, close to the resolution limit.

Following X-ray radiography, the welded plates were sectioned for mechanical testing and metallography as shown in Fig. 3.

Metallography and Microstructural Analysis

All metallographically evaluated weld specimens were sectioned transverse to the weld direction and mounted in clear resin. Standard metallographic techniques were employed in the preliminary preparation of the specimens. Final polishing, however, involved alternate polishing with 0.3μ Linde A and etching in a 50% picric and 50% nital solution. This technique was found to yield maximum contrast and resolution from weld and HAZ (Heat Affected Zone) microstructures as well as from the inclusions. Inclusion count and size measurements were performed on optical micrographs taken at 45X magnification with a Leitz pan-phot microscope. At 45X magnification, it was necessary to compose a large composite micrograph of each section from series of smaller individual micrographs in order to resolve at least 10μ size inclusions and still view the entire weld profile.

Elemental qualitative and quantitative analysis was performed on selected specimens using a Cameca scanning electron microprobe. X-ray and back scatter techniques were employed to establish the identity of weld and base metal inclusions. In addition, a point count analysis was performed to determine the precise quantity of weld and base metal aluminum. All findings were based on analysis of at least three different areas.

Hardness measurements of weld, HAZ and base metal were obtained using a Shimadzu Seisakusha microhardness tester with a 500 gm load. Four measurements were taken from each of the three areas with average values recorded below.

Mechanical Testing

Mechanical test specimens were taken from welded plates as indicated in Fig. 3. Typical tensile, bend and Charpy impact specimens are shown in Fig. 4.

Bend Testing

Bend test bars were taken traverse to the weld bead. Root bend specimens were fabricated and tested according to the method described in ASTM E190-64 (Ref. 5). After bending, the convex surfaces of the welds were examined for cracks and open defects by a light microscope and by magnetic particle techniques (the Magnaflux technique). The welds were magnafluxed with the field imposed both parallel to and normal to the weld direction.

Tensile Testing

The circular cross section of the tensile specimens was centered relative to the plate thickness and the weld bead location was centered along the longitudinal axis of the specimen. Specimens were tested in a Tinius-Olsen four screw testing machine at 70°F (21.1°C) at a strain rate of 0.01 in./in./min (1.67×10^{-4} cm/cm/sec). Fabrication and testing of tensile specimens was done according to the methods described under ASTM E8-69 (Ref. 6).

Charpy Impact Tests

Charpy impact test specimens were centered relative to the plate thickness. Half-size specimens were fabricated from the 0.64 cm and 0.95 cm plates while full-sized specimens were fabricated from the 1.27 cm plate. The parent metal and weld specimens were obtained from the same segment cut from each plate (see Fig. 3). Notches for all specimens were oriented along the welding direction and, for the weld specimens obtained from the 0.95 cm and 1.27 cm plates, the

notches were centered in the weld zone. Notches in the weld specimens from the 0.64 cm plate were located in three locations throughout the weld and heat affected zones as can be seen in the photograph in Fig. 4. Fabrication and testing of Charpy impact specimens were conducted in accordance with the methods prescribed in ASTM E23-72 (Ref. 7).

For the 30°F (-1.4°C) tests, specimens were placed in a dewar containing a salt, ice and water bath maintained at 30°F. After immersion at temperature for a minimum period of ten minutes, specimens were removed from the bath using tongs, refrigerated in the same dewar, placed in the impact machine and tested within a maximum of 15 seconds after removal from the bath. A typical time from bath to impact was well under ten seconds. A 264 ft-lb (357 joule) capacity Tinius-Olsen impact tester was used, and was carefully calibrated before and after each series of tests.

Dynamic Tear Tests

Unnotched subsized dynamic tear specimens were forwarded to the Naval Research Laboratories, Washington, DC (NRL). The facilities at NRL are more experienced at machining the special notches required and are better equipped to conduct the actual tests. Test procedure will follow a technique proposed for a 0.625 in. (16 mm) thick specimen. The dimensions for a 0.625 in. specimen and subsized specimens are shown in Table III. Conversion of data obtained on subsized samples to 0.625 dynamic tear energy by means of a sizing factor. The sizing factors are also shown in Table III. Testing procedures are indicated in Ref. 8.

RESULTS AND DISCUSSION

Initial work on the laser welded HY-130 plates involved NDT characterization and destructive testing of the welds to determine their properties as compared to the base metal. In addition, extensive quantitative metallographic examination was conducted in order to clarify and quantify the observed reductions in the inclusion content of the material following laser welding. These striking reductions are believed to be an important element in maintaining excellent mechanical properties in the laser welds without extensive attempts to control heating and cooling rates which are dictated by the autogenous laser process.

Nondestructive Testing (Visual and Radiographic Examination)

Following welding, all plates were visually inspected and were classified as to the weld bead appearance. Further inspection was accomplished by X-ray radiography. The combined results of the X-ray and visual inspections are summarized in Table IV. Positive prints of the weld X-rays are shown in Figs. 5-7. It can be seen from the table and figures that conditions were readily established for welding of the 0.64 cm thick plate with reproducibly clean, uniform, and porosity-free welds. Welds in the 0.95 cm thick plate were typically the poorest of the three thicknesses studied. In studying the nature of the inclusions in all plate thicknesses, it was found that the 1.27 cm thick plate investigated was rare-earth treated, whereas the 0.64 and 0.95 cm thick plates investigated were deoxidized by conventional means. Since it would be expected that the difficulty in producing good welds would normally increase with increasing material thickness, it appears that the rare-earth treatment greatly influences the weld quality. This will be discussed further below, in light of the mechanical test results.

Weld Bead Cross Sections

Bead profiles for the welds listed in Table IV were determined by cross sectioning the welds at the locations schematically indicated in Fig. 3 and designated "M" on the radiographs in Figs. 5-7, polishing and etching, and photographing these etched cross sections. Representative cross sections of the "A" series welds (0.64 cm thick plate) are shown in Fig. 8, while those of the "B" series (0.95 cm thick plate) and the "C" series (1.27 cm thick plate) are shown in Figs. 9 and 10. It can be seen that the beads in the A series consisted of two types, closely tied to the power levels. Specimens A-1 through A-3 showed narrow beads with excessive undercut in A-1 and A-3. This undercut was not severe at the slowest welding speed A-2. All three specimens were somewhat overpenetrated and showed "broadening" in the center section, a situation

which often leads to porosity, as was the case with these welds. When the power was reduced to 6 kW (A-4 through A-8) and the speed reduced proportionately, a broader weld zone with a continuing taper was produced and undercut was eliminated in all cases except A-7, where the plates were, unfortunately, poorly matched. Specimens welded at 6 kW also exhibited a somewhat larger grain size than those fabricated at 10 kW, a situation which, due to the slower cooling rate which produced this effect, would be somewhat beneficial to impact resistance, but which would be slightly unfavorable regarding the ductile/brittle transition temperature. X-ray radiographic results (Table IV) identified the welds produced more slowly at the 6 kW level as having substantially better integrity than those fabricated at 10 kW.

The beads fabricated in the B series are displayed in Fig. 9. The initial weld, B-1 was excessively narrow as a result of the high welding speed, whereas B-2 which was fabricated substantially more slowly exhibited substantial "broadening" at the plate center which is undesirable as discussed above. The profiles of welds B-3 through B-6 appeared to be close to optimum, however excessive porosity was encountered in these welds due to factors which are believed to be related to deoxidation practice. (The section of weld B-4 displayed in Fig. 9 was taken too close to the "starting defect" and is not characteristic of the equilibrium weld shape.) The best apparent cross section was B-5 which also radiographed the best overall, although there are two pores visible in the section displayed in Fig. 9. Some "nontypical" situations have occurred in the displayed sections as discussed above because these sections were taken close to the ends of the test welds (see Fig. 3) so that the major portion of the plate could be available for further testing.

The C series welds (Fig. 10) began with C-1 which was welded slightly too rapidly, and, although a reasonable appearing bead was produced, proved to be excessively porous. The welding speed of C-2 was clearly too high, and the dual-pass weld C-3 was unsuccessful due to the high degree of root porosity in the second or "blind" pass. Welds C-2 and C-3 were sufficiently poor that no further mechanical tests were conducted on these samples. Welds C-4 through C-9 were significantly better and were close to what was felt to be optimum within the limitations of available laser power for these tests. All of these welds had somewhat "broadened" centers, a situation which is nonoptimum for total elimination of porosity, and, in fact, the welds did contain some porosity, although less, on the whole, than the B-series. It is felt that with additional laser power which would allow a larger spot without reducing incident power density, a longer focal length could be employed to produce a slightly wider, continuously tapering weld, without severe porosity. On the whole, the welds in this series were still a bit too narrow to be optimum from the porosity standpoint.

Mechanical Test Results

Bend Tests

Bend test results are summarized in Fig. 11, which shows typical root bend specimens for each of the three thicknesses of laser-welded HY-130 plate. The data from these tests including inspection results is summarized in Table V. Bends in the 0.64 and 0.95 cm plate were made to the standard 3t radius. No failures were noted, and consequently, bends in the 1.27 cm plate were made to a more severe 2t radius. Even in this case, no failures were observed. Following bending, the specimens were visually inspected and found to have no cracks. To insure the absence of cracks, magnaflux testing was also used. Magnaflux tests were conducted with fields oriented for cracks both parallel and perpendicular to the welds. All specimens were found to be completely free of cracks in the welds and surrounding regions.

Microhardness Measurements

Microhardness traverses were completed on the six specimens for which inclusion content and size distribution were characterized. These values are tabulated in Table VI. In all cases the highest hardnesses were observed in the heat affected zones, and averaged R_c 43.2 as compared to the base metal average of 34.4. The weld fusion zones exhibited intermediate values averaging R_c 39.8. This hardness is characteristic of the behavior of laser-welded ferrous alloys at similar carbon levels due to the cooling rate increases inherent in the laser welding process. Higher tensile strengths in the welds are expected, but questions involving the impact resistance in Charpy and dynamic tear tests must be answered to insure that adequate toughness of the welds accompanies these higher strengths.

Tensile Tests

Circular cross section cross-weld tensile specimens were tested to failure with no failures occurring in the weld regions, heat affected zones, or regions adjacent to the heat affected zones. The welds, having cooled more rapidly than the base plate were clearly stronger than the base alloy. Thus, no weld failures were anticipated except in cases where the welds may have been seriously weakened by flaws. The absence of weld tensile failures attests to the absence of mechanically serious flaws within the laser welds over the entire thickness range investigated. The tensile test results are summarized in Table VII. A photograph of failed tensile bars appears in Fig. 12. Since all tensile specimen failures occurred remote from the weld zone, it was concluded that weld tensile strength exceeded base metal tensile strength for all welding conditions.

Tensile test results, as applied to the base plate indicated that the 0.95 cm thick plate (B series) had significantly higher ultimate tensile strength than either the 0.64 cm or 1.27 cm thick plates. This coincides with the observed higher base-metal inclusion content and lower base metal impact strengths which are noted and discussed below. The additional inclusions apparently provide a strengthening effect, however the toughness is somewhat reduced as a result of these extra inclusions. Tensile ductility was found to be highest for the cleaner, higher toughness, rare-earth treated 1.27 cm thick plate, which would be expected, however, the fact that the elongation of the 0.95 cm thick plate was slightly greater than that of the 0.25 cm thick plate is presently unexplained.

Impact Tests

Weld and base metal impact specimens from the laser-welded plates were tested at two temperatures, 70°F (21.1°C) and 30°F (-1.4°C). The welding conditions for these plates were summarized in Table III and their impact values are tabulated in Table VIII.

It can be seen from the data in Table VIII that the impact resistance of all welds in the 0.64 cm thick plate was equal to or greater than that of the base metal. Interestingly, there were two distinct base metal impact strength levels, indicating that there was a major and important difference in metallurgy between the various as-received plates of 0.64 cm HY-130 stock which were provided for the study. Gross differences in inclusion content had previously been noted in metallography, giving rise to the opinion that the plates used to fabricate specimens A-3, A-6 and A-8 and having base line Charpy impact strengths averaging 54.6 joules, were most probably rare-earth treated, whereas the plates used to fabricate the remaining weld samples and having Charpy impact values averaging 36.9 joules were not. This is presently being verified by the electron microprobe. The Charpy values measured in the base metal were not widely scattered, but fell into two close groupings, giving support to the above theory. Weld metal impact values in the 0.64 cm plate closely followed parent material values with specimen A-8 being the single exception. Weld A-8, however, was not shielded on the root side due to an error in its fabrication.

In the 0.64 cm material, since the welds exhibited good quality in X-ray radiography, notches were placed in three different locations in an effort to evaluate these three areas. Notch locations included the weld center line, the heat affected zone, and a location within the fusion zone halfway between these locations. The data on specimens A-1 through A-6 where notch positions were varied systematically, clearly indicated that there was no major difference in properties of notched impact specimens as a function of location within the weld

and HAZ. The two HAZ-notched values did appear to be a bit lower than those produced by the other notch locations, but they are certainly not significantly different. All 0.64 cm welds including specimen A-8 which was not properly shielded appeared to meet Navy requirements for HY-130 weld impact toughness, although A-8 was the only value below the parent metal as a result of the fabrication error.

The intermediate thickness 0.95 cm thick welds did not, on the whole, exhibit good quality. Most of these welds exhibited considerable steady porosity as evidenced by the X-rays in Fig. 5 and their interpretations in Table V. Despite this apparent difficulty in welding, other mechanical properties as measured in tensile and bend tests did not appear to be problematic. During the course of the investigation, however, no welding parameters capable of producing porosity-free, or even nearly porosity-free welds were found, and so the 0.95 cm thick welds were tested despite their known internal flaws. Surprisingly, Charpy impact strengths, as exhibited in Table VIII were almost all equivalent to or better than the base metal values. The one notable exception was specimen B-4 which registered a 17 percent decrease in impact resistance. All others were within 10 percent and several were greater with the average parent metal value being 31.7 joules, somewhat less than the weld average of 32.6 joules. Base metal values for the 0.95 cm plate were all consistent and were lower than the lower group of values in the 0.64 cm plate, indicating that the overall metallurgical quality of the 0.95 cm plate was not as high as for the thinner material. This factor, along with the greater plate thickness was felt to be responsible for the increased difficulty in welding this thickness and the fact that only porous welds were produced. If thickness were the key element, it would be expected that the 1.27 cm material would prove even more difficult to weld, however the X-rays (Fig. 6) and observations in Table IV attest to the fact that better welds were made at this thickness. The base metal impact values on all of the 1.27 cm plates were high as compared to the other thicknesses (except for the specifically high-valued 0.64 cm material), and it was ultimately confirmed by electron microprobe analysis that the 1.27 cm thick material was rare-earth earth treated. In this thicker, rare-earth treated material, a significant decrease in weld metal impact strength was observed with the base metal averaging 151.3 joules and the welds averaging 106.0 joules. This indicates that, when the base metal's metallurgical quality is sufficiently high, it is not possible to improve it enough through the localized refinement and purification which occur during laser welding (as detailed below) to compensate for the reduction in impact strength which naturally accompanies more rapid quenching in alloy steels, and which produces increased tensile and yield strengths, and higher hardness. It is, however, significant to note that the 106 joule average Charpy impact value is considerably in excess of the normally required average Charpy impact value of 74.4 joules for the -1.4°C-21.1°C temperature range. Table VIII

indicates, also, that even the lowest impact value, 80.7 joules, which occurred in a weld which was far from optimum, exceeds the required value. In addition to purely metallurgical factors, it should be remembered that the welds were not physically perfect, having a certain amount of porosity. The relative extent to which porosity influences the impact strength compared to metallurgical factors is not quantitatively known, but qualitatively, it appears to be small, and this has been verified by other studies (Ref. 10).

In an effort to define somewhat more clearly the relative importance of metallurgical and physical factors, experiments have been planned which include reducing the thicknesses of the original 1.27 cm thick plate and 0.95 cm thick plate to 0.95 and 0.64 cm respectively. We can then weld 0.95 plate with a better rare earth-treated metallurgical structure and compare it to the apparently lowest quality 0.95 cm plate welded and reported upon above. In addition, we will reduce some of this poor 0.95 cm plate to 0.64 cm and see how the laser welds made at that thickness compare with those already fabricated in the somewhat better apparent quality (but not rare-earth treated) 0.64 cm plate above. These experiments are planned to shed additional light on the importance of metallurgical quality on ability to autogenously laser weld and on the importances of both the metallurgical quality and physical quality of the weld on its impact resistance. In addition, fractography is being performed on the impact fractures and is planned for the dynamic tear specimens discussed below in another effort to sort out the relative roles of physical and metallurgical factors.

Dynamic Tear Tests

The dynamic tear test results are summarized in Table IX. These tests were performed at the U. S. Naval Research Labs under the direction of Dr. Ed Metzbower.

It can be seen in Table IX that the dynamic tear energies for the 0.25 in. (0.64 cm) specimens were uniformly high, ranging from 123 to 193 ft-lbs (167 j). Using sizing factors as reported by Brenna and McCaw (Ref. 11), this would convert to 1150-1803 ft-lbs (1559-2444 j) in a 5/8 in. (1.59 cm) dynamic tear specimen or 10,350-16,227 ft-lbs (14,029-21,994 j) in a 1 in. (2.54 cm) dynamic tear specimen. These values considerably exceed the highest base metal values on the RAD diagram, and although the tests conclude that the specimens were obviously quite tough, the results are not considered fully "valid" as a result of the unduly small specimen thickness. The value for specimen A-3 is unrealistically high probably because of failure to reset the dynamic tear machine before this test and was thus eliminated. Likewise, the value for A-8 is too low and was suspect because no notch depth is shown. The B specimens, 3/8 in. (0.95 cm) thick also showed good values, but not as high, as the 1/4 in. (0.64 cm). These specimens exhibited some porosity and occasionally substantial porosity, but still showed DT energies in the middle of the normal base

metal range. The average value, converted to a 1 in. specimen was 5580 ft-lbs (7563 j), which is actually above the middle of the range indicated on the RAD diagram. The specimen size was marginal, and so the "validity" of these tests cannot be fully assured.

The half inch (1.27 cm) specimens showed ductile DT fractures as clearly indicated in Fig. 13, and were considered to be "fully valid test specimens". The values for these specimens, as shown in Table X, were again equivalent to the high end of the normal base-metal range for HY-130 steel; 6698 ft-lbs (9077 j) average. Values for specimens C-1 and C-9 were negatively influenced because of excessive porosity. The results of the dynamic tear testing of HY-130 alloy have thus shown the layer welds in this study in all thicknesses to be highly tough and fracture resistant. A detailed analysis of these DT tests, including fractographic observations, is planned, with the results to be distributed in the form of a separate report because of their highly significant nature as far as the Navy's current interests in laser welding are concerned.

Quantitative Analysis of Metallurgical Structure

Inclusion count and size measurements, and electron beam microprobe analyses were performed on two samples from each of the three thickness categories of laser-welded HY-130 steel plate. All specimens were observed at 45 magnifications, and samples were selected based on the numbers of inclusions of 10μ in diameter or above. The "best case" and the "worst case" in each thickness category were chosen for investigation with the "best case" (bc) being the weld with the fewest resolvable inclusions and the "worst case" (wc) being the weld with the greatest number of resolvable inclusions within a given thickness category. As indicated in Table X and clearly documented in Figs. 14-19, all three specimen thicknesses exhibited marked reduction in resolvable weld inclusion content (10μ resolution limit) as compared with an immediately adjacent equal area of base metal. This was true for both "best cases" and "worst cases", as well as for all plate thicknesses. (Note: Reduction in magnification of the original photomicrographic maps which required encircling of inclusions for clarity in Figs. 14-19.) The percentage of resolvable inclusions retained in each case is also given in Table X. In the best noted example of fusion zone purification (1.27 cm or "c" plate), 82 percent of the resolvable inclusions were eliminated from the weld fusion zone during the process of deep penetration laser welding. In the worst observed example involving the "A" plate, 44 percent of the resolvable inclusions were eliminated. Investigation of the inclusion count data in Table X surprisingly indicated a trend toward greater fusion zone purification with increased specimen thickness. Although this effect was not predicted, it is most probably explained by the fact that the thicker sections require greater specific energy inputs, allowing more time for inclusions

to be vaporized and aspirated from the weld. The proposed physical mechanism for fusion zone purification during deep penetration laser welding is explained in Ref. 2.

Table XI contains the results of an inclusion size distribution study, and indicates that the effects of laser welding on inclusion size within the resolvable range were uncertain. For example, in the 0.64 cm plate, one specimen exhibited a major (68.6%) decrease in maximum inclusion size, while the other specimen exhibited a sizable (60%) increase. There was, however, an overall trend towards a minor reduction in weld fusion zone inclusion size as compared to the base metal. These data favor explanation of weld properties as a result of eliminating inclusions, rather than simply refining them.

Results of electron beam microprobe analysis of inclusion compositions are given in Table XII. X-ray patterns for representative inclusions of the two characteristic types found are shown in Figs. 20 and 21. The microprobe analysis revealed the presence of two distinct types of inclusions. The inclusions found in the samples of 0.64 and 0.95 cm plate were all aluminum oxides with small amounts of adhering free calcium (Fig. 20). All of the inclusions found in the 1.27 cm thick plate were lanthanum/cerium oxides (Fig. 21), indicating that this thicker plate was rare-earth treated. No rare-earth oxide inclusions were found in the A and B plates, and no aluminum oxides were found in the C plates. (Although impact testing subsequently revealed that some of the 0.64 cm thick plate had high impact resistance and was probably rare-earth treated, it happened that the two 0.64 cm specimens selected for microprobe analysis using the "best and worst case" criterion were both lower impact resistance specimens and so contained only inclusions of the Al-O + Ca type. The presence of rare earths in the other specimens is presently being verified.) Although numerous inclusions were sampled in each of the six selected specimens, no other types of inclusions were found in either the welds or the base metal.

In an effort to establish what happened to the inclusions which were eliminated from the weld fusion zones of a specimen characterized by the Al/O type of inclusion, a quantitative electron microprobe analysis was performed on weld and base metal. Results of the analysis failed to show any increase of aluminum in the matrix (noninclusion area) of the weld fusion zone, and, in fact, revealed a small decrease. It was apparent from these data that the constituents of the missing inclusions were, most likely, not retained in the welds. A similar determination for oxygen was made previously and was reported in Ref. 2. This gives added support to the mechanism of inclusion removal previously proposed in Ref. 2 which involves preferential vaporization of nonmetallic inclusions as a result of their preferential absorption of the 10.6μ CO_2 laser radiation, and aspiration of these vaporized inclusions from the deep penetration cavity.

SUMMARY OF RESULTS AND CONCLUSIONS

1. Three series of test welds were produced in HY-130 alloy steel plate provided by the U. S. Navy DTNSRDC. Three thicknesses of plate were welded, 0.64 cm, 0.95 cm, and 1.27 cm. Laser powers ranged from 6.0 to 12.8 kW, with welding speeds between 1.27 and 2.96 cm/sec.

2. All welds were visually inspected, X-rayed, and mechanically tested in bending, tension, impact, and dynamic tear. Weld, HAZ, and base metal hardness and microstructure were also evaluated, and bend test specimens were also magnafluxed following testing.

3. X-ray examination revealed that welds in 0.64 cm thick material were "X-ray clear". Welds in the 0.95 cm plate were typically the poorest, with severe porosity in a variety of distributions. Welds in the 1.27 cm thick plate were of considerably better quality than those of the thinner 0.95 cm plate, exhibiting sparse, fine porosity in most cases.

4. The nature of the inclusions in the 1.27 cm thick plate indicated that this material was rare-earth treated, which accounted for the better "weldability" of this thicker material.

5. Weld beads in all thicknesses exhibited acceptable cross sections with only an occasional tendency for "widening" at the center of the bead. Root and face reinforcements were adequate in almost all cases. It was possible to produce adequate bead shapes following suitable parameter adjustment in all cases.

6. All 0.64 cm and 0.95 cm thick weld specimens survived 3t guided bend tests without failure. The 1.27 cm thick specimens survived 2t guided bend tests, also without failure. All specimens were magnafluxed, and no cracks were found following bend tests.

7. Microhardness measurements revealed the average weld fusion-zone hardness to be R_c 39.8. HAZ hardness was highest, at R_c 43.2 compared to average base metal hardness of R_c 34.4.

8. Tensile test specimens did not fail in the welds. UTS values ranged from 961 to 1076 MPa with elongations from 12.0 to 15.7%. Strength and ductility values within the three thickness categories related to observed base-metal inclusion content.

9. Impact values in the 0.64 cm thick plate, as measured at two temperatures, were all in excess of base metal. In the 0.95 cm material, although there was considerable porosity, nearly all impact values were equivalent to base metal or higher. In the rare-earth treated 1.27 cm material, impact values were uniformly below the base metal, due to a high base metal level, but all values were substantially in excess of Navy specifications for HY-130 welds at the two temperatures.

10. Dynamic tear test results in all thicknesses were at the high end of base metal HY-130 values as indicated on Navy RAD diagrams. Though the validity of the 0.64 cm and 0.95 cm tests is doubtful due to "specimen size effects", the 1.27 cm tests were felt to be fully valid. The dynamic tear tests serve to highlight the high fracture toughness which can be achieved in HY-130 laser welds.

11. Quantitative analysis of HY-130 laser weld structures showed decreases in resolvable (10μ) inclusion content ranging from 44 to 82 percent considering all three thicknesses welded and the best and worst case in each thickness, thoroughly documenting the fusion zone purification effect in these welds.

12. A trend toward greater purification with increasing plate thickness was noted. This trend was not anticipated. A plausible explanation based on increased specific energy input with thickness was proposed.

13. Studies of the inclusion size distribution indicated that the effects of fusion zone purification during laser welding on the inclusion size distribution were uncertain.

14. Electron beam microprobe analysis indicated inclusions in the 0.64 and 0.95 cm thick plates to be aluminum oxides with small amounts of calcium, indicating conventional deoxidation practice. In the 1.27 cm thick plate, lanthanum/cerium oxides were predominant, indicating rare-earth treatment.

15. Quantitative electron beam microprobe analysis of weld and base metal in the 0.64 and 0.95 cm thick plates failed to show any increase of aluminum in the matrix (noninclusion area) of the fusion zone, indicating that the constituents of the missing inclusions were most likely not retained in the welds.

16. Based on the above results, it was concluded that the laser welding process is capable of making acceptable and mechanically excellent welds in HY-130 alloy steel through 1.27 cm thickness. Weldability of the alloy is improved by better deoxidation practice (rare earth treatment) although substantial elimination of inclusions by the Fusion Zone Purification effect was observed and quantitatively verified in all cases of laser welding encountered in this study.

REFERENCES

1. Breinan, E. M. and C. M. Banas, "Evaluation of Basic Laser Welding Capabilities", Technical Report, Contract N00014-74-C-0423, United Technologies Research Center, East Hartford, CT, Nov. 1975.

2. Breinan, E. M. and C. M. Banas, "Fusion Zone Purification During Welding with High Power CO_2 Lasers", Proceedings of the Second International Symposium of the Japan Welding Society, Osaka, Japan, Aug. 24-28, 1975.

3. Breinan, E. M. and C. M. Banas, "Preliminary Evaluation of Laser Welding of X-80 Arctic Pipeline Steel", Welding Research Council Bulletin #201, Dec. 1974.

4. Brown, C. O., et al, "Investigation of a High Power CO_2, Convection Laser", Report L910990-22, United Technologies Research Center, Final Report under Navy Contract N60921-70-C-0219 sponsored by the Naval Ordnance Systems Command, May 1972.

5. ASTM E190-64, Standard Method for Guided Bend Test for Ductility of Welds. 1976 Annual Book of ASTM Standards, Part 10, ASTM, Philadelphia, PA, 1976.

6. ASTM E8-69, Standard Methods of Tension Testing of Metallic Materials. 1976 Annual Book of ASTM Stnadards, Part 10, ASTM, Philadelphia, PA, 1976.

7. ASTM E23-72, Standard Methods for Notched Bar Impact Testing of Metallic Materials, 1976 Annual Book of ASTM Standards, Part 10, ASTM, Philadelphia, PA, 1976.

8. Proposed Method for 5/8 in. (16 mm) Dynamic Tear Test of Metallic Materials. 1976 Annual Book of ASTM Standards, Part 10, ASTM, Philadelphia, PA, 1976.

9. Brown, C. O. and C. M. Banas, "Deep Penetration Laser Welding", paper presented at the AWS 52nd Annual Meeting, San Francisco, CA, Apr. 26-29, 1971.

10. Banas, C. M. and G. T. Peters, "Study of the Feasibility of Laser Welding in Merchant Ship Construction", Final Report to Bethlehem Steel on their Contract 2-36214 with the U. S. Department of Commerce, Aug. 1974.

11. McCaw, R. L. and R. T. Brenna, "Specimen Size Effects in Mechanical Property Testing of HY-130 Steel", Report TM-28-75-74, DTNSRDC, Materials Department, Fabrication Technology Div., Ferrous Welding Branch, Code 2821, Annapolis, MD.

Table I

Nominal Composition of HY-130 Alloy Steel

Element	Wt Percent
Fe	Bal
C	0.09-0.11
Mn	0.25
Cr	0.50
Mo	0.40
V	0.07
Ni	5.50

Table II

HY-130 Welding Conditions Investigated

Series A 1/4 in. (0.64 cm) Thick Material

Sp #	Welding Power-kW	Welding Speed (in./min)	(cm/sec)
A-1	10.0	70	2.96
A-2	10.2	60	2.54
A-3	10.0	80	3.39
A-4	6.0	40	1.69
A-5	6.0	40	1.69
A-6	6.0	40	1.69
A-7	6.0	40	1.69
A-8	6.0	40	1.69

Series B 3/8 in. (0.95 cm) Thick Material

B-1	10.0	50	2.12
B-2	10.0	30	1.27
B-3	10.0	40	1.69
B-4	10.0	40	1.69
B-5	10.0	40	1.69
B-6	10.0	40	1.69

Series C 1/2 in. (1.27 cm) Thick Material

C-1	12.8	40	1.69
C-2	12.2	50	2.12
C-3	12.0	128*	5.42*
C-4	10.0	30	1.27
C-5	10.0	30	1.27
C-6	10.0	30	1.27
C-7	10.0	30	1.27
C-8	10.0	30	1.27
C-9	10.0	30	1.27

*Dual pass weld attempted from two sides (128 in/min (5.42 cm/sec) each side)

Table III

Dynamic Tear Test Specimen Size

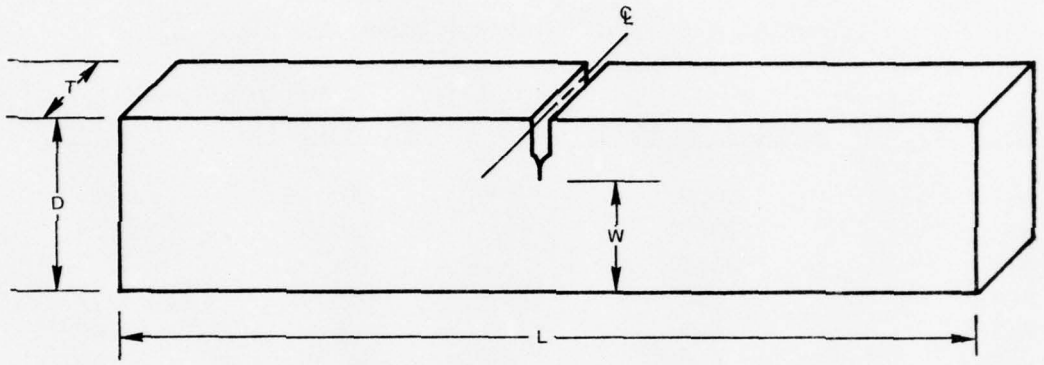

T (in.)	D (in.)	L (in.)	W (in.)	Sizing Factor ($W^2\sqrt{T}$)
0.625	1.625	7.0	1.125	1.0000
0.5	1.625	7.0	1.00	0.7071
0.375	1.250	7.0	0.750	0.3445
0.250	1.000	7.0	0.500	0.1250

Table IV

Visual and X-Ray Inspections of HY-130 Laser Welds

Specimen #*	Power (kW)	Speed (cm/sec)	Inspection Results
A-1	10.0	2.96	Scattered porosity
A-2 best case	10.2	2.54	Scattered porosity, some nonuniformity of bead, step offset between plates
A-3	10.0	3.39	Isolated, grouped porosity, some undercut & underbead spatter
A-4	6.0	1.69	Excellent apparent weld quality
A-5 worst case	6.0	1.69	Excellent apparent weld quality
A-6	6.0	1.69	Good, but not quite as good as A-5
A-7	6.0	1.69	Excellent apparent weld quality
A-8	6.0	1.69	Porosity-free. Ineffectively shielded on the back side.
B-1	10.0	2.12	Severe, uniformly distributed porosity
B-2	10.0	1.27	Heavy, fairly uniformly distributed porosity
B-3 worst case	10.0	1.69	Fairly heavy, medium-sized porosity throughout. Uneven bead, Poor metal flow at end of weld
B-4	10.0	1.69	Initially heavy porosity, then intermittent. End of weld is good
B-5 best case	10.0	1.69	Various sizes of pores along entire length
B-6	10.0	1.69	Relatively free from porosity. Some lack of fusion & "choppy" bead
C-1 worst case	12.8	1.69	Considerable porosity (some large) and spatter
C-2	12.2	2.12	Severe porosity along entire length
C-3	12.0	5.42 dual pass	Fine line of root porosity & some sizable pores
C-4	10.0	1.27	Isolated porosity - rest of weld is good

Table IV (Cont'd)

Specimen #*	Power (kW)	Speed (cm/sec)	Inspection Results
C-5	10.0	1.27	Porosity near end, instability at start, center okay
C-6	10.0	1.27	Generally good with separated porosity
C-7	10.0	1.27	Sparse porosity only
C-8	10.0	1.27	Large porosity, shielding was marginal
C-9	10.0	1.27	Ends not fully shielded, isolated pores

* "A" specimens 0.64 cm thick, "B" specimens 0.95 cm thick, "C" specimens 1.27 cm thick

Table V

Summary of Bend Test Results

Specimen No.	Nominal Plate Thickness (cm)	Width (cm)	Bend Radius	Loading Rate cm/sec	Maximum Load	Magnaflux Inspection*
A-1	0.64	1.27	3t	.004	7153	Crack free
A-2	↓	↓	↓	↓	6779	↓
A-3	↓	↓	↓	↓	6726	↓
A-4	↓	↓	↓	↓	7420	↓
A-5	↓	↓	↓	↓	7099	↓
A-6	↓	↓	↓	↓	7313	↓
A-7	↓	↓	↓	↓	6566	↓
A-8	↓	↓	↓	.021	6939	↓
B-1	0.95	1.91	3t	.021	26690	Crack free
B-2	↓	↓	↓	↓	26160	↓
B-3	↓	↓	↓	↓	26160	↓
B-4	↓	↓	↓	↓	25350	↓
B-5	↓	↓	↓	↓	24820	↓
B-6	↓	↓	↓	↓	25350	↓
C-1	1.27	2.54	2t	.004	59380	Crack free
C-2	↓	-	↓	-	-	↓
C-3	↓	-	↓	-	-	↓
C-4	↓	2.54	↓	.021	58050	↓
C-5	↓	↓	↓	↓	58050	↓
C-6	↓	↓	↓	↓	58050	↓
C-7	↓	↓	↓	↓	57380	↓
C-8	↓	↓	↓	↓	58050	↓
C-9	↓	-	↓	↓	-	↓

*Fields oriented to reveal cracks both parallel to and perpendicular to the welds

Table VI

HY-130 Laser Weld Hardness Values

Sample No.	R_c Hardness Weld Fusion Zone	Heat Affected Zone	Base Metal
A-5 (T)	39.8	44.5	33.3
A-2	41.3	44.5	36.5
B-5	40.2	42.9	35.5
B-3	38.8	41.8	33.5
C-1	39.3	42.9	33.4
C-7	39.9	42.7	34.5

Table VII

Results of Tensile Tests on Laser-Welded HY-130 Steel

Specimen No.	Specimen Diameter	UTS (Kpsi)	UTS (MPa)	% Elongation
A-1	0.125	143	984	15.0
A-2	0.128	139	958	12.0
A-3	0.128	140	964	13.9
A-4	0.127	141	973	12.0
A-5	0.128	140	964	12.1
A-6	0.127	141	973	12.5
A-7	0.127	142	980	13.7
A-8	0.126	141	969	12.4
B-1	0.188	156	1076	13.4
B-2	0.187	154	1062	13.5
B-3	0.188	155	1069	14.1
B-4	0.187	154	1062	13.7
B-5	0.188	153	1058	13.3
B-6	0.188	152	1051	13.0
C-1	0.250	143	983	14.5
C-4	0.251	139	961	14.5
C-5	0.252	140	962	14.9
C-6	0.251	141	970	14.6
C-7	0.251	141	970	15.7
C-8	0.252	141	970	14.6
C-9	0.252	142	979	15.2

Table VIII

Results of Charpy V-Notch Impact Tests on
Laser-Welded HY-130 Plates

Specimen No.	Test Temp (°C)	Parent Metal Location (joules/ft-#)	Notch Location in Weld	Weld Metal Impact (joules/ft-#)	Comments
A-1*	21.1	35.2/26.0*	HAZ	32.5/24.0*	
A-2	-1.4	38.0/28.0	HAZ/WELD	37.3/27.5	
A-3	21.1	51.5/38.0	HAZ/WELD	53.6/39.5	
A-4	-1.4	36.6/27.0	WELD ℄	36.6/27.0	
A-5	21.1	37.3/27.5	WELD ℄	48.8/36.0	
A-6	-1.4	53.6/39.5	HAZ	50.8/37.5	
A-7	21.1	37.2/27.5	WELD ℄	37.2/27.5	
A-8	21.1	58.8/43.5	WELD ℄	38.5/28.5	Weld not shielded on back
B-1*	21.1	32.5/24.0*	WELD ℄	35.2/26.0*	
B-2	-1.4	29.2/21.5	WELD ℄	41.4/30.5	
B-3	21.1	31.2/23.0	WELD ℄	31.2/23.0	
B-4	-1.4	31.9/23.5	WELD ℄	26.4/19.5	
B-5	21.1	33.1/24.5	WELD ℄	29.2/23.5	
B-6	21.1	32.5/24.0	WELD ℄	29.7/22.0	
C-1	21.1	156.6/115.5	WELD ℄	106.4/78.5	
C-2	-				Poorest welds, no specimens fabricated
C-3	-				
C-4	21.1	146.4/108.0	WELD ℄	80.7/59.5	
C-5	-1.4	153.9/113.5	WELD ℄	104.4/77.0	
C-6	21.1	147.8/109.0	WELD ℄	109.2/80.5	
C-7	-1.4	149.8/110.5	WELD ℄	124.1/91.5	
C-8	21.1	150.1/111.0	WELD ℄	123.0/91.0	
C-9	21.1	154.8/114.5	WELD ℄	94.0/69.5	

*Half-size specimens used due to plate thickness

Table IX

Dynamic Tear Test Results - HY-130 Laser Welds

Specimen No.	T(in)	W(in)	$W^2\sqrt{T}$	Notch Depth (in)	Double-Pendulum DT Energy (ft-lb)	(j)	Equivalent DT Energy 5/8" Specimen (ft-lb)
A-1	.179	.502	.107	.017	123	167	1150
A-2	.177	.504	.107	.011	123	167	1150
A-3	.183	.503	.108	.007	668*	905	6185*
A-4	.186	.505	.110	.011	176	239	1600
A-5	.185	.504	.109	.012	186	252	1706
A-6	.180	.503	.107	.010	193	262	1803
A-7	.182	.503	.108	.013	182	247	1685
A-8	.180	.506	.109	-	47**	64	431**
B-1	.334	.751	.330	.017	142	192	430
B-2	.333	.751	.325	.009	142	192	436
B-3	.335	.753	.328	.008	164	222	500
B-4	.322	.753	.322	.011	281	381	872
B-5	.322	.751	.320	.012	326	442	1018
B-6	.327	.752	.323	.008	150	203	464
C-1	.465	.998	.679	.009	404	548	595
C-4	.459	.996	.672	.011	562	762	836
C-5	.470	.997	.681	.012	637	863	935
C-6	.455	.997	.671	.020	442	599	659
C-7	.459	.998	.675	.008	546	740	809
C-8	.462	.998	.677	.019	455	617	672
C-9	.461	.997	.675	.008	374	507	554

*Machine probably not reset

**No notch depth recorded

Table X

Inclusion Counts for Equivalent Weld Fusion Zone and Base Metal Areas

(10μ minimum resolvable inclusion size)

Sample No.	Best or Worst Case	Inclusion Count		Percentage of Inclusions Retained
		Weld Fusion Zone	Base Metal	Weld/Base
A-5(T)	BC	39	120	32.4
A-2	WC	51	91	56.0
B-5	BC	18	36	50.0
B-3	WC	100	324	31.0
C-1	WC	74	302	24.5
C-7	BC	12	67	18.0

Table XI

Range of Inclusion Sizes for HY-130 Laser
Weld Fusion Zones and Base Metal

Sample No.	Inclusion Size Range (μ) Weld Fusion Zone	Base Metal
A-5(T)	10-25	10-67
A-2	10-40	10-25
B-5	10-15	10-30
B-3	10-35	10-40
C-1	10-50	10-50
C-7	10-20	10-30

Table XII

Principal Elements Comprising Inclusions in
HY-130 Base Metal and Laser Welds

(Electron Beam Microprobe Analysis)

Sample No.	Inclusion Composition	
	Weld Fusion Zone	Base Metal
A-5(T)	-	-
A-2	Al-Ca-O	Al-Ca-O
B-5	-	-
B-3	Al-Ca-O	Al-Ca-O
C-1	La-Ce-O	La-Ce-O
C-7	La-Ce-O	La-Ce-O

HIGH POWER LASER WELD FIXTURING

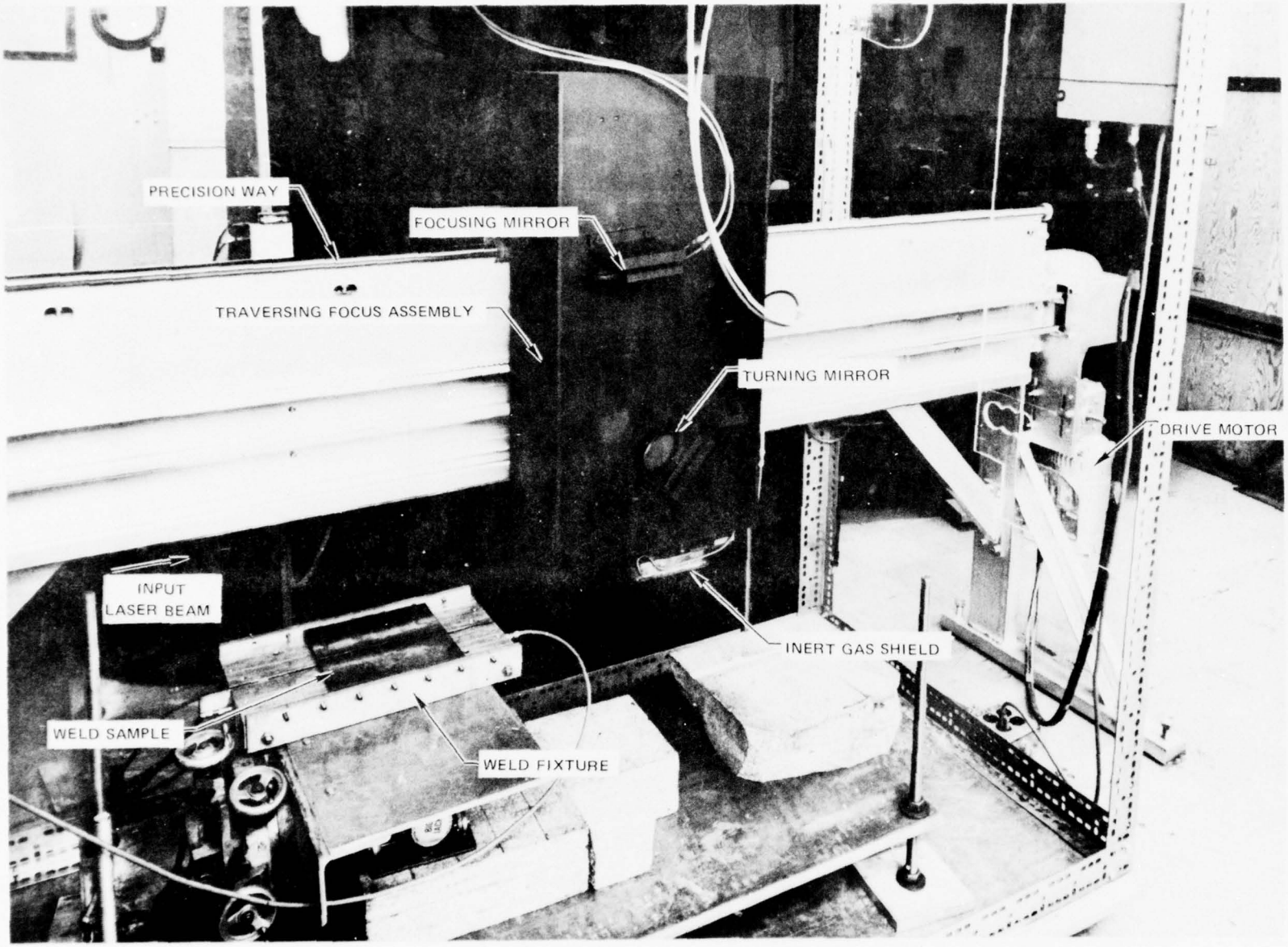

R77-911989-10

FIG. 1

RL-74-167-F

N06-129-2

R77-911989-10

SCHEMATIC DRAWING OF HY-130 LASER WELD FIXTURING AND GAS SHIELDING

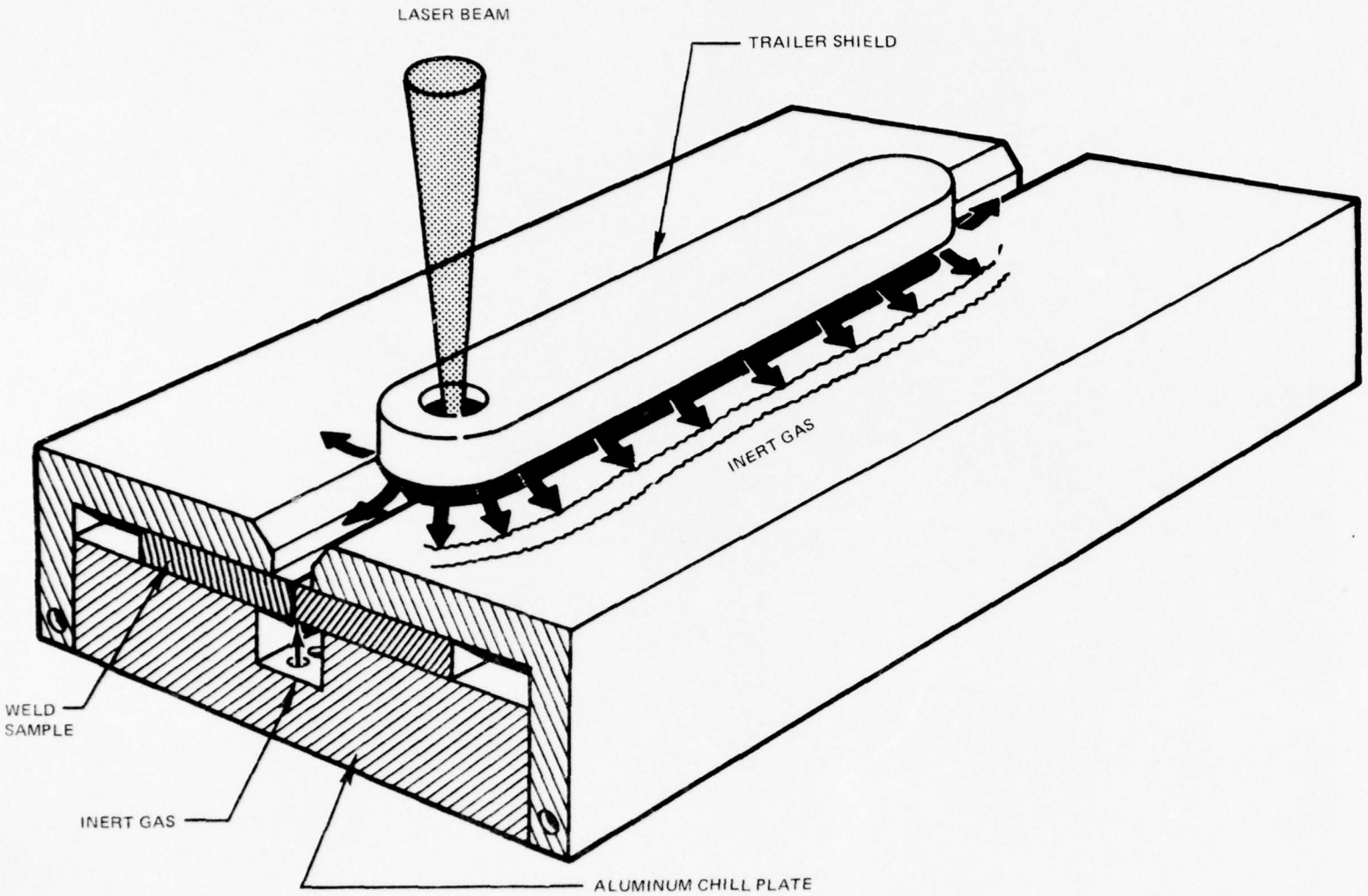

FIG. 2

77-01-272-3

SECTIONING OF TYPICAL HY–130 LASER WELD TEST PLATE FOR MECHANICAL TESTING AND METALLOGRAPHY

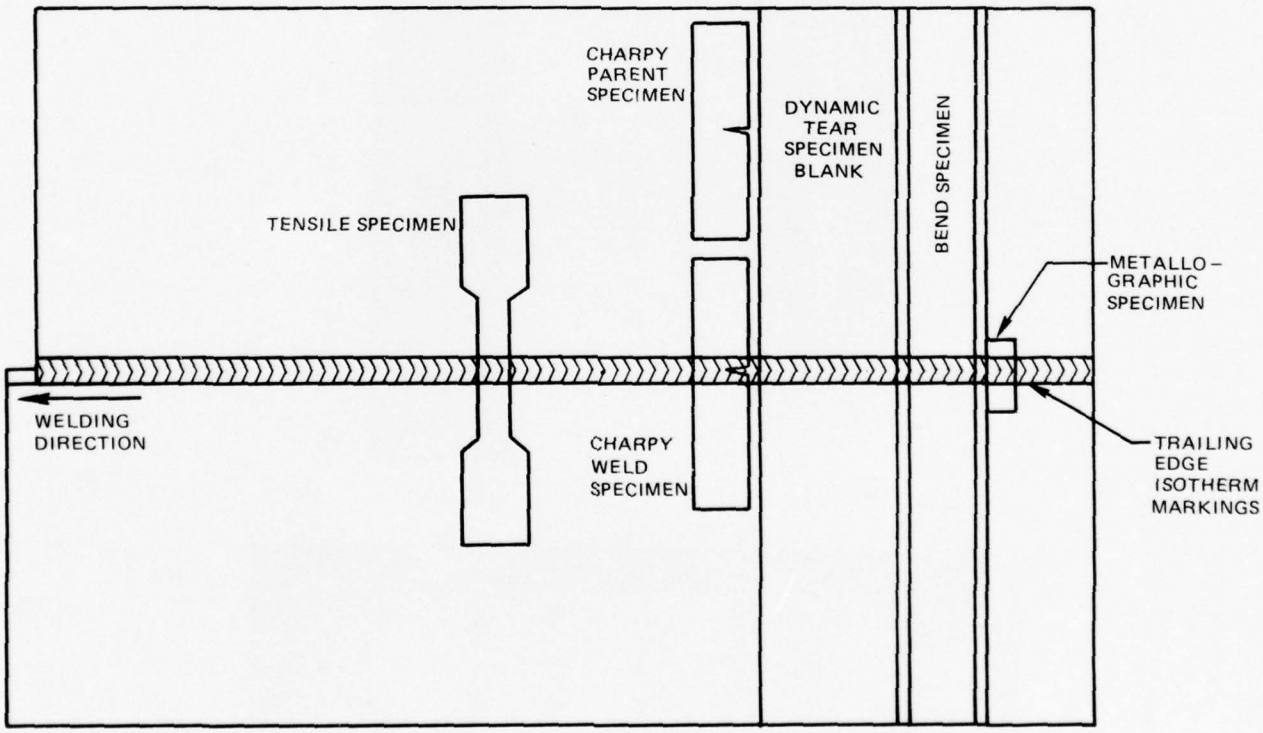

77–02–19–4

MECHANICAL TEST SPECIMENS OF HY–130 LASER WELDS

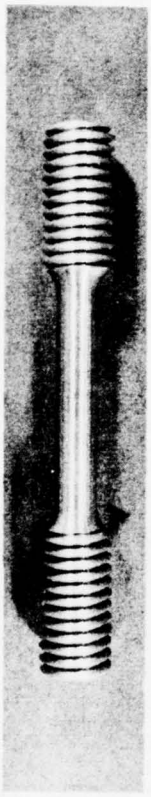

TENSILE SPECIMEN ~ 1 X

BEND SPECIMEN ~ 1/2 X

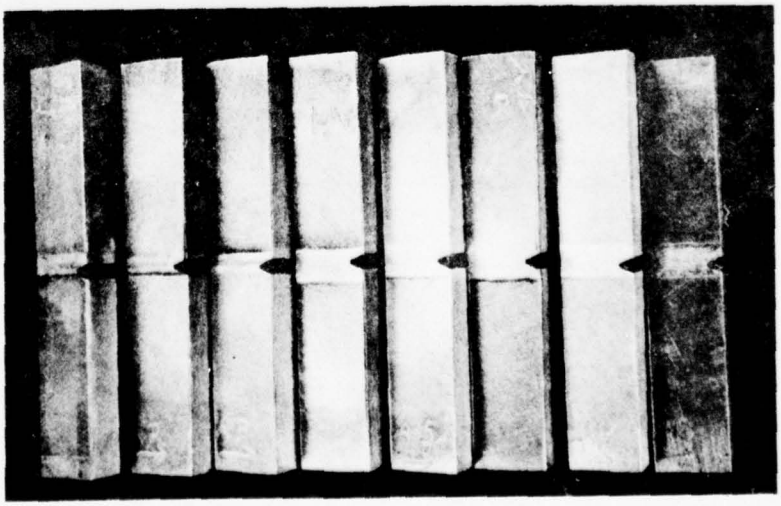

CHARPY IMPACT SPECIMENS FROM 0.64 ON THICK PLATE SHOWING NOTCHES ON WELD ℄ AND IN FUSION ZONE AND HAZ

FIG. 5

RADIOGRAPHS OF LASER WELDS IN 0.64 CM THICK HY–130 STEEL

(ACTUAL SIZE)

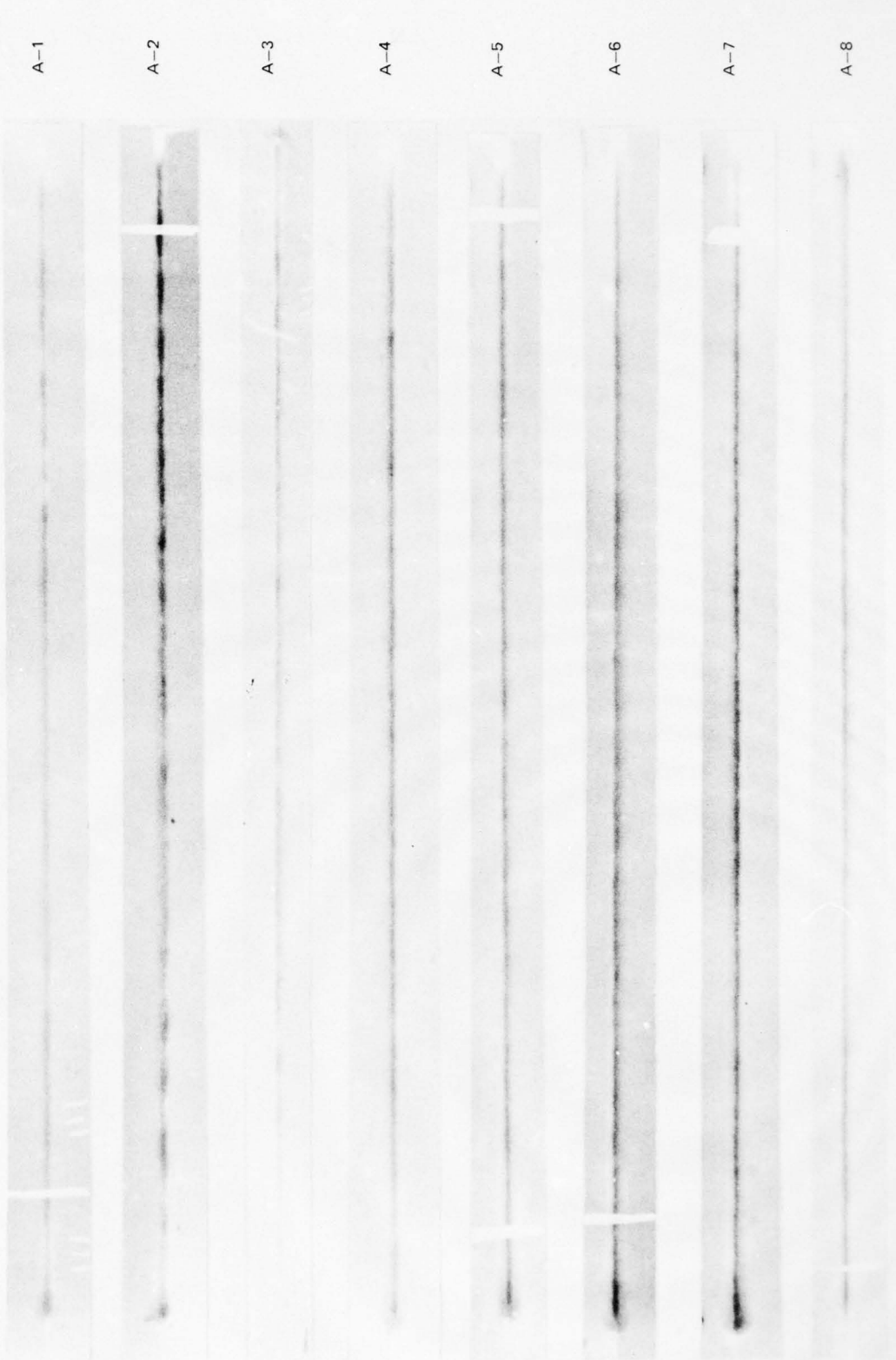

FIG. 6

RADIOGRAPHS OF LASER WELDS IN 0.95 CM THICK HY–130 STEEL

(ACTUAL SIZE)

FIG. 7

RADIOGRAPHS OF LASER WELDS IN 1.27 CM THICK HY–130 STEEL

(ACTUAL SIZE)

CROSS SECTIONS OF LASER WELDS IN 0.64 CM THICK HY–130 STEEL

4X MAGNIFICATION

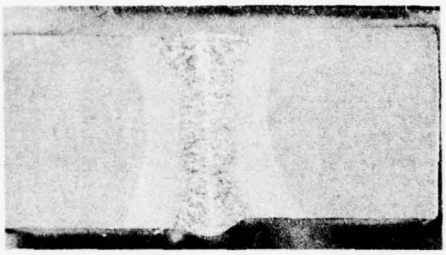

A–1

A–2

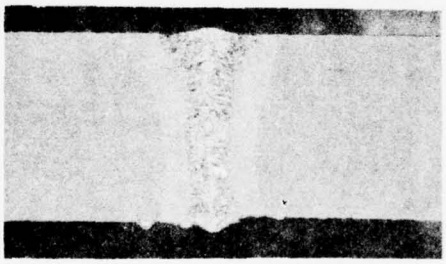

A–3

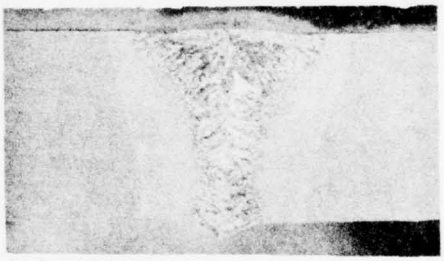

A–4

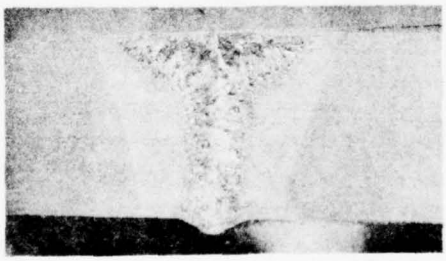

A–5

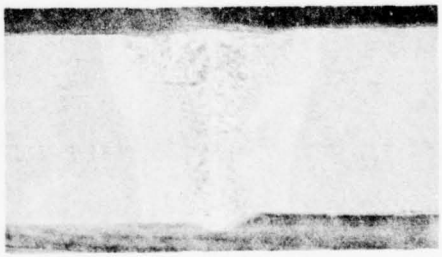

A–6

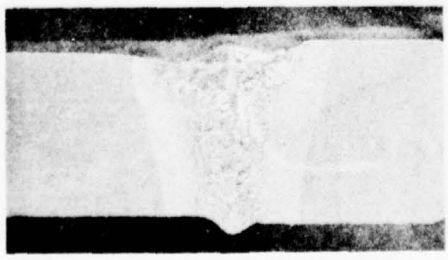

A–7

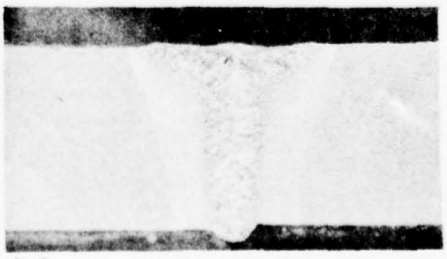

A–8

CROSS SECTIONS OF LASER WELDS IN 0.95 CM THICK HY–130 STEEL

7.5X MAGNIFICATION

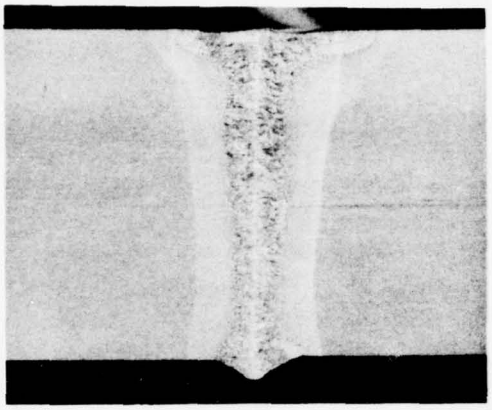

B–1

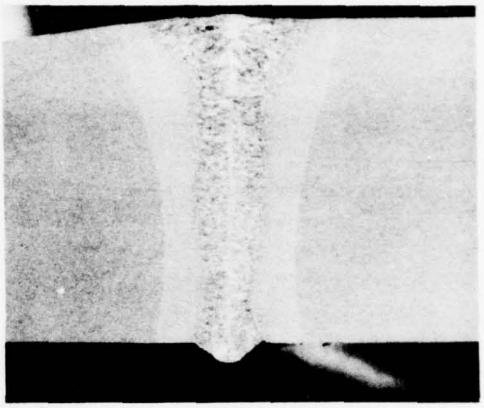

B–2

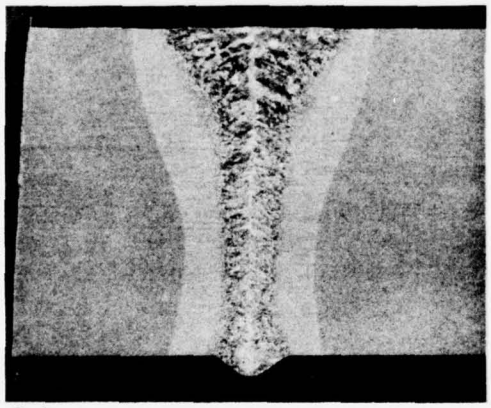

B–3

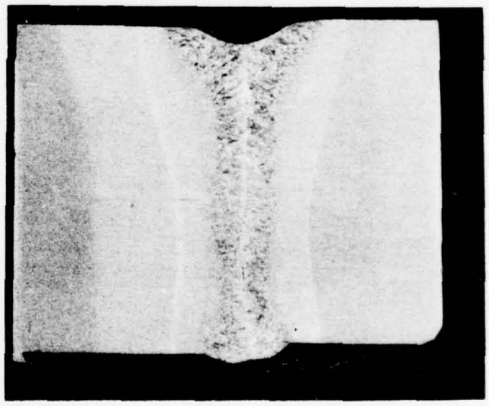

B–4

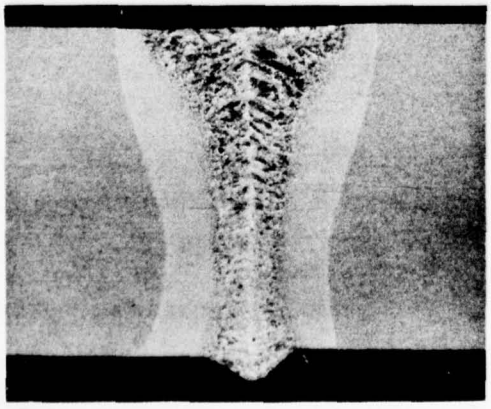

B–5

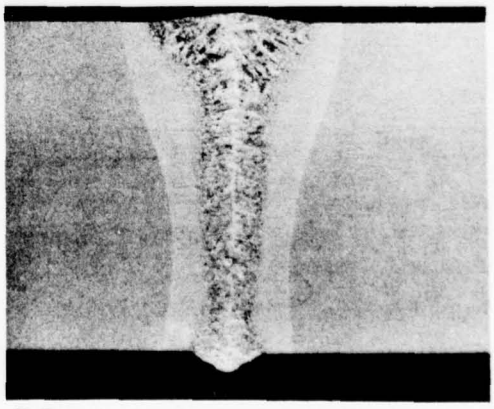

B–6

R77–911989–10

FIG. 10

CROSS SECTIONS OF LASER WELDS IN 1.27 CM THICK HY–130 STEEL

5X MAGNIFICATION

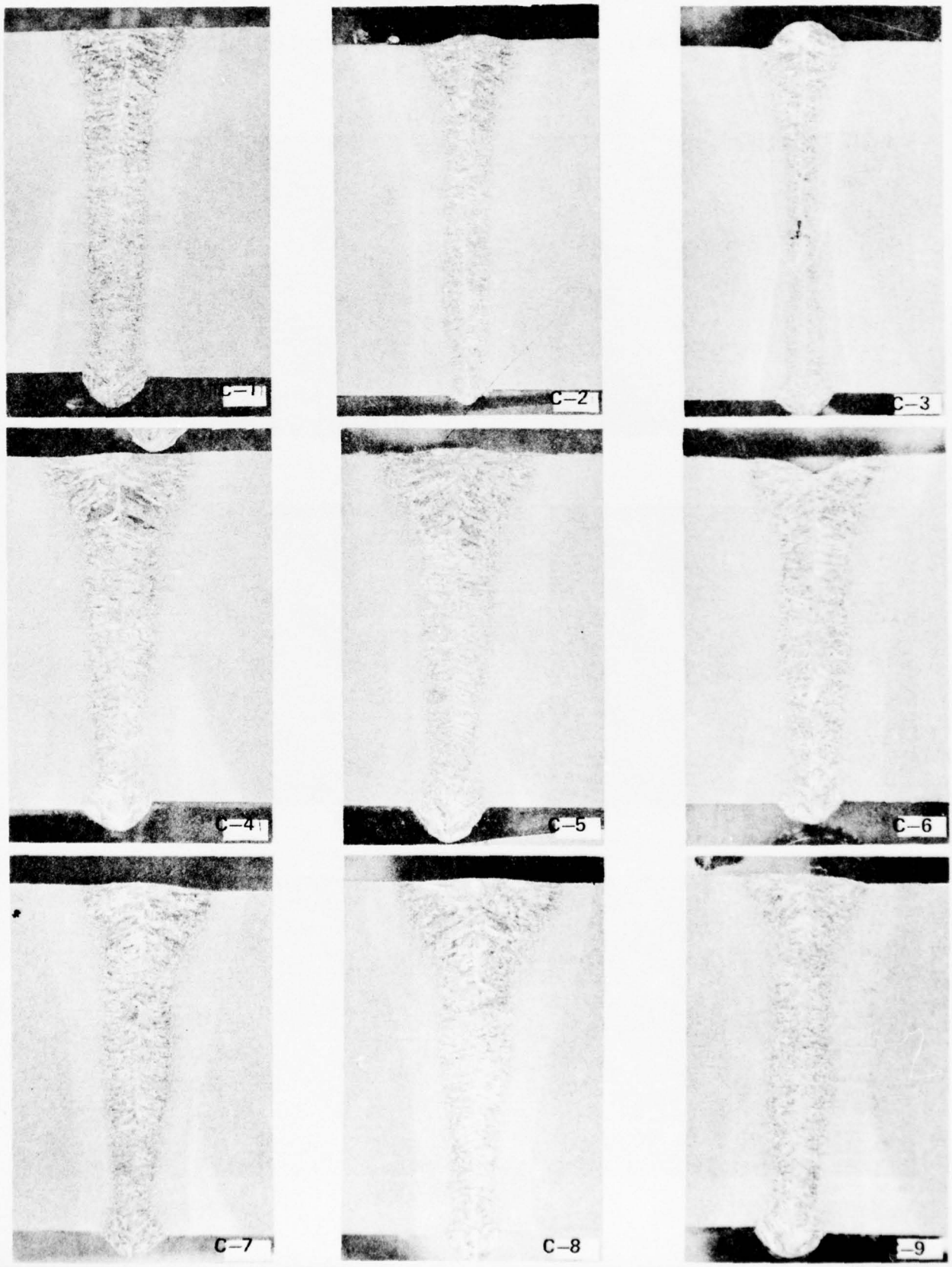

77–02–4–3

TYPICAL RESULTS OF BEND TESTS ON THREE THICKNESSES OF LASER WELDED HY-130 STEEL PLATE

NOTE: NO CRACKS WERE DETECTED BY MAGNAFLUX EXAMINATION

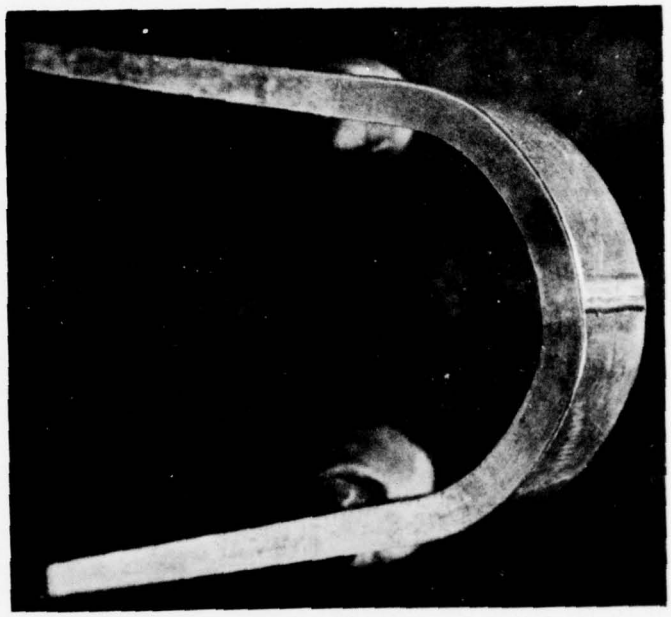

0.64 CM THICK PLATE ~ 1 X

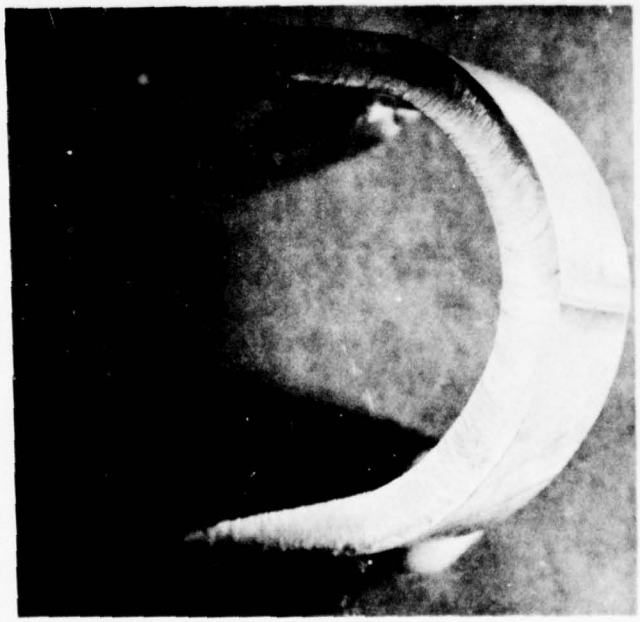

0.95 CM THICK PLATE ~ 1 X

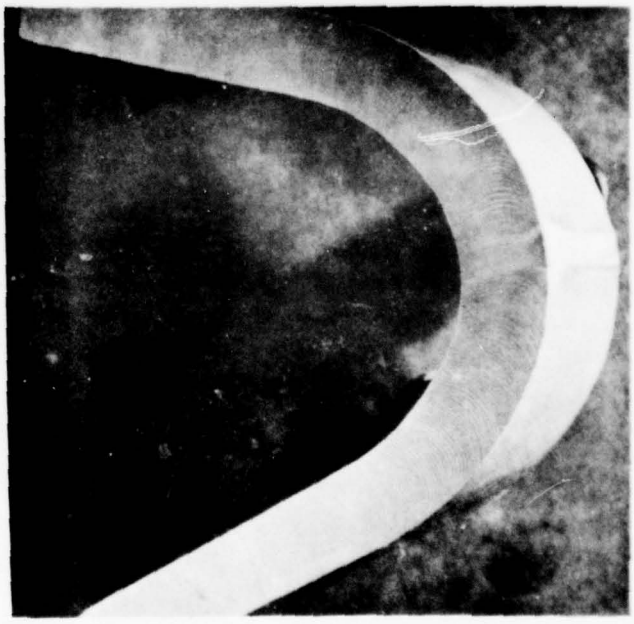

1.27 CM THICK PLATE ~ 1 X

TYPICAL HY-130 LASER WELD TENSILE SPECIMENS FOLLOWING TESTING

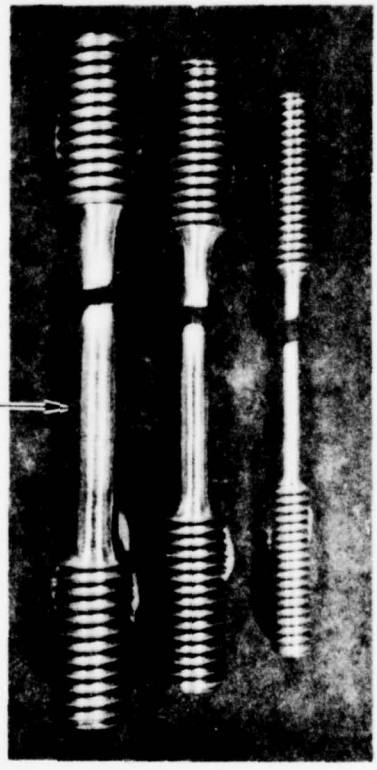

~ 1X

DYNAMIC TEAR SPECIMEN OF 1.27 CM THICK LASER-WELDED HY-130 PLATE

(APPROXIMATELY ACTUAL SIZE)

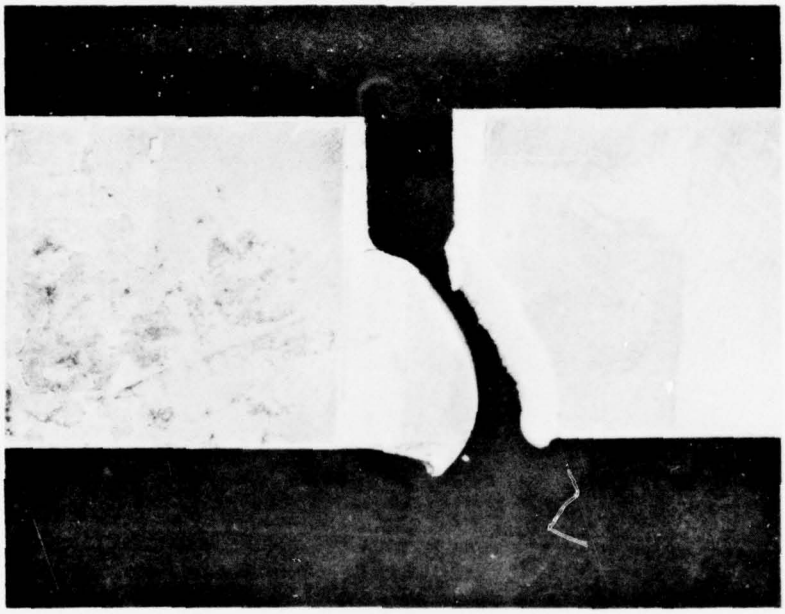

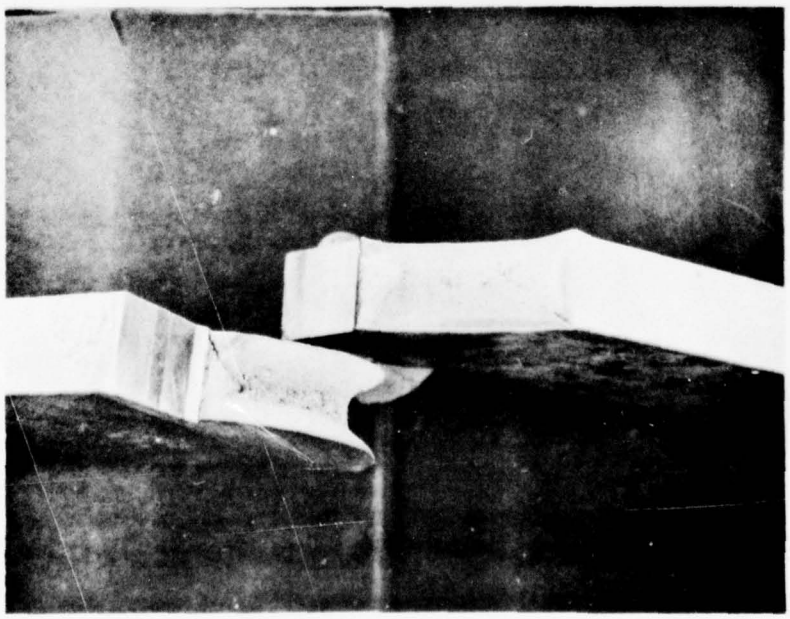

77-02-266-1

R77–911989–10

DISTRIBUTION OF INCLUSIONS IN THE WELD FUSION ZONE AND EQUIVALENT ADJACENT

BASE METAL – 120 INCLUSIONS WELD FUSION

(NOTE: REDUCTION IN MAGNIFICATION FROM ORIGINAL PHOTOGRAPHIC MAP R

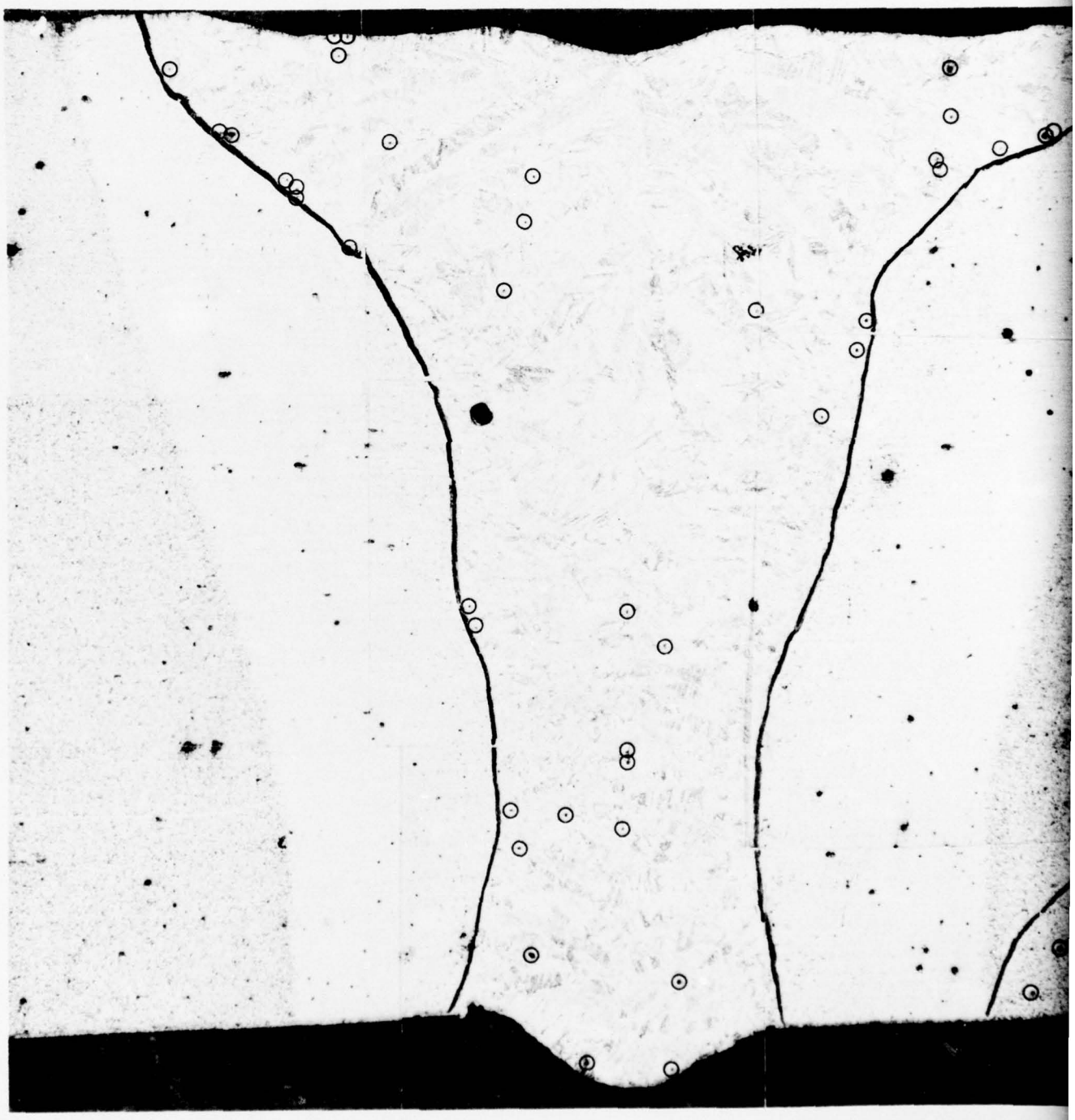

FIG. 14

VALENT ADJACENT AREA OF BASE METAL IN HY–130 LASER WELD SPECIMEN A–5

IS WELD FUSION ZONE – 39 INCLUSIONS

L PHOTOGRAPHIC MAP REQUIRED ENCIRLING OF INCLUSIONS FOR CLARITY)

500 μ

R77–911989–10

DISTRIBUTION OF INCLUSIONS IN THE WELD FUSION ZONE AND EQUIVALENT ADJACENT

BASE METAL – 91 INCLUSIONS WELD FUSION Z

(NOTE: REDUCTION IN MAGNIFICATION FROM ORIGINAL PHOTOGRAPHIC MAP REC

R77–911989–10

DISTRIBUTION OF INCLUSIONS IN THE WELD FUSION ZONE AND EQUIVALENT ADJACENT AR

BASE METAL – 36 INCLUSIONS WELD FUSION ZON

(NOTE: REDUCTION IN MAGNIFICATION FROM ORIGINAL PHOTOGRAPHIC MAP REQU

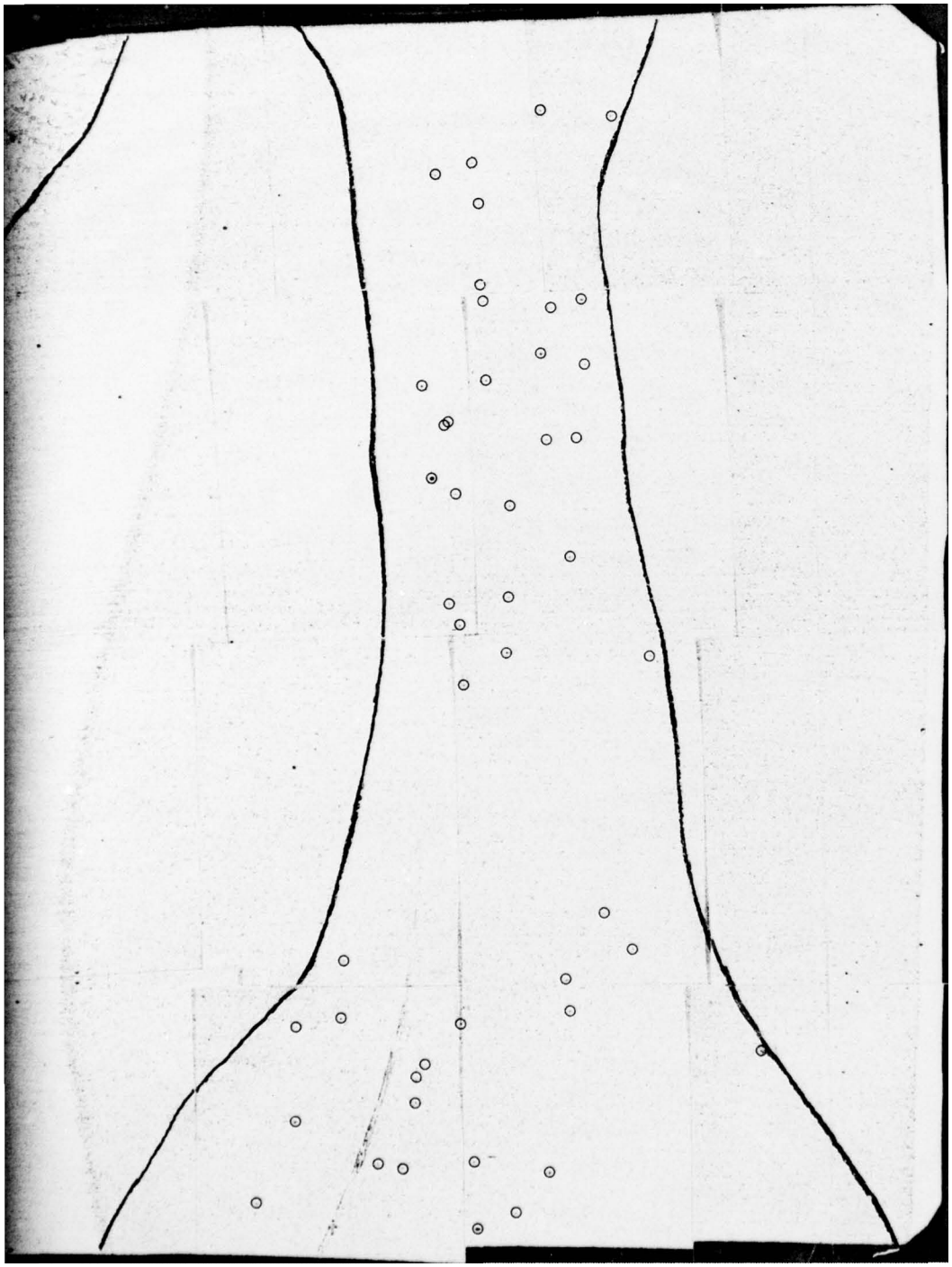

R77–911989–10

DISTRIBUTION OF INCLUSIONS IN THE WELD FUSION ZONE AND EQUIVALENT ADJACENT AR

BASE METAL – 324 INCLUSIONS WELD FUSION ZON

NOTE: REDUCTION IN MAGNIFICATION FROM ORIGINAL PHOTOGRAPHIC MAP REQU

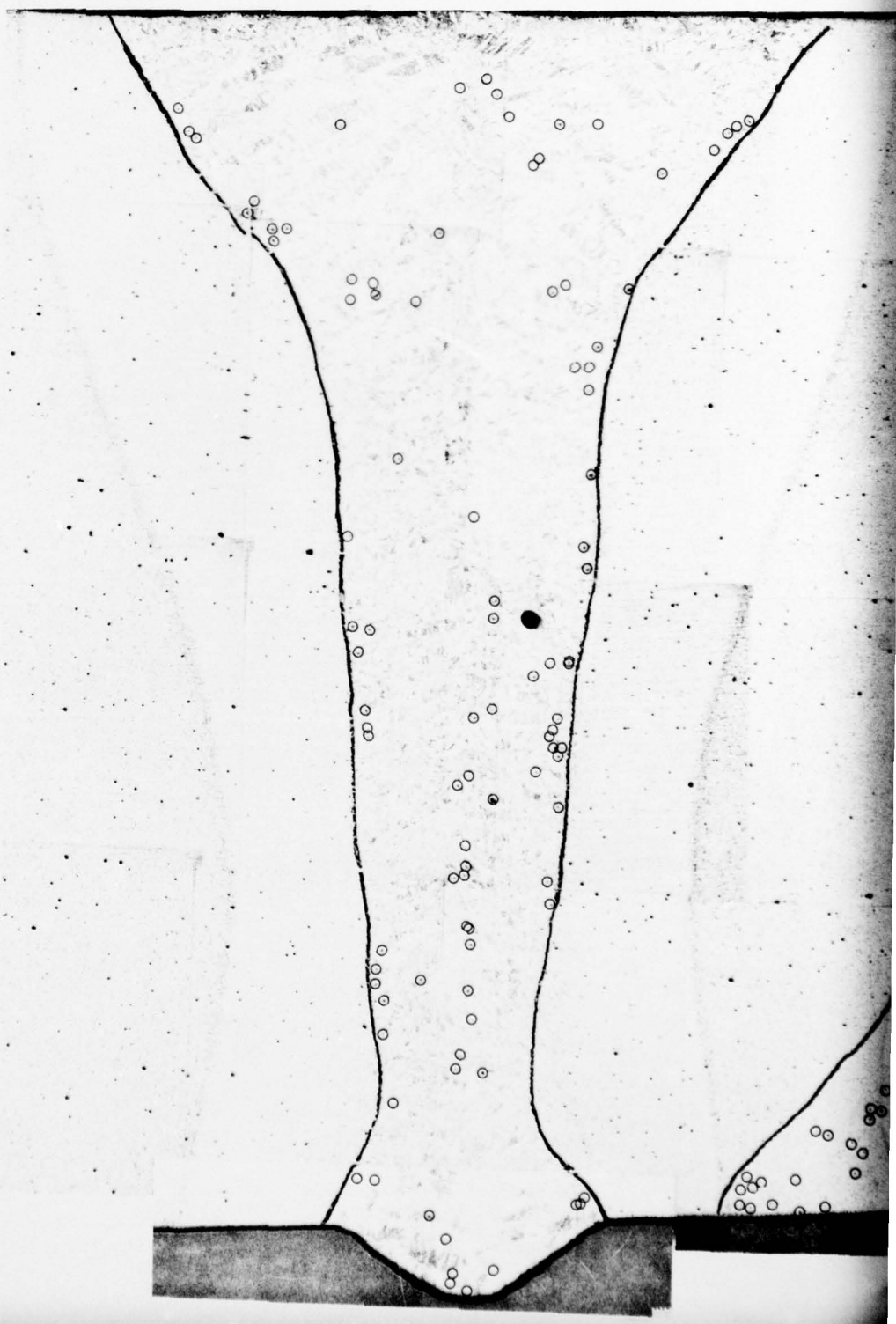

FIG. 17

EQUIVALENT ADJACENT AREA OF BASE METAL IN HY–130 LASER WELD SPECIMEN B–3

CLUSIONS WELD FUSION ZONE – 100 INCLUSIONS

ORIGINAL PHOTOGRAPHIC MAP REQUIRED ENCIRCLING OF INCLUSIONS FOR CLARITY.)

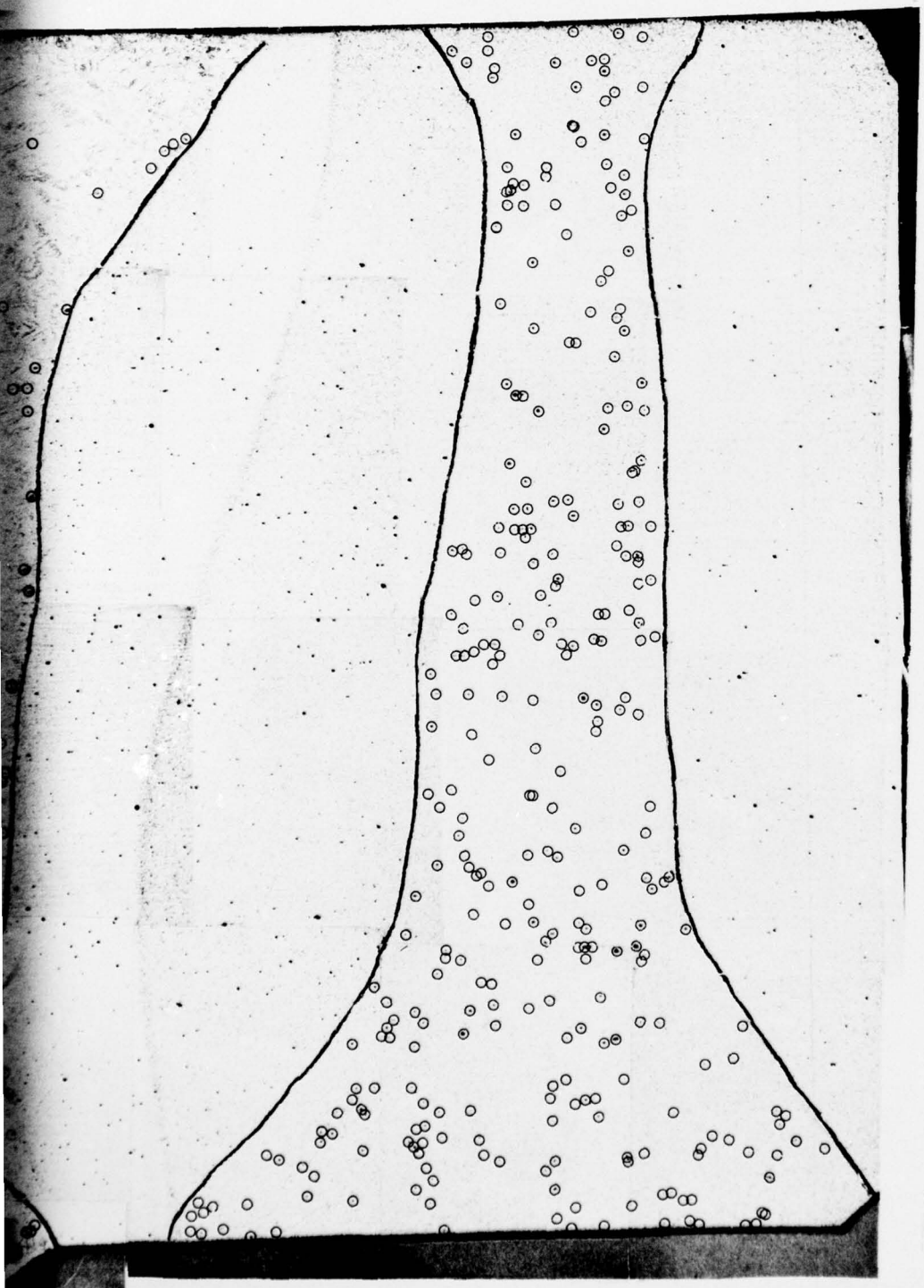

R77–911989–10

DISTRIBUTION OF INCLUSIONS IN THE WELD FUSION ZONE AND EQUIVALENT ADJACENT A

BASE METAL – 302 INCLUSIONS WELD FUSION ZO

(NOTE: REDUCTION IN MAGNIFICATION FROM ORIGINAL PHOTOGRAPHIC MAP REQ

FIG. 18

NT ADJACENT AREA OF BASE METAL IN HY–130 LASER WELD SPECIMEN C–1

WELD FUSION ZONE – 74 INCLUSIONS

OGRAPHIC MAP REQUIRED ENCIRCLING OF INCLUSIONS FOR CLARITY.)

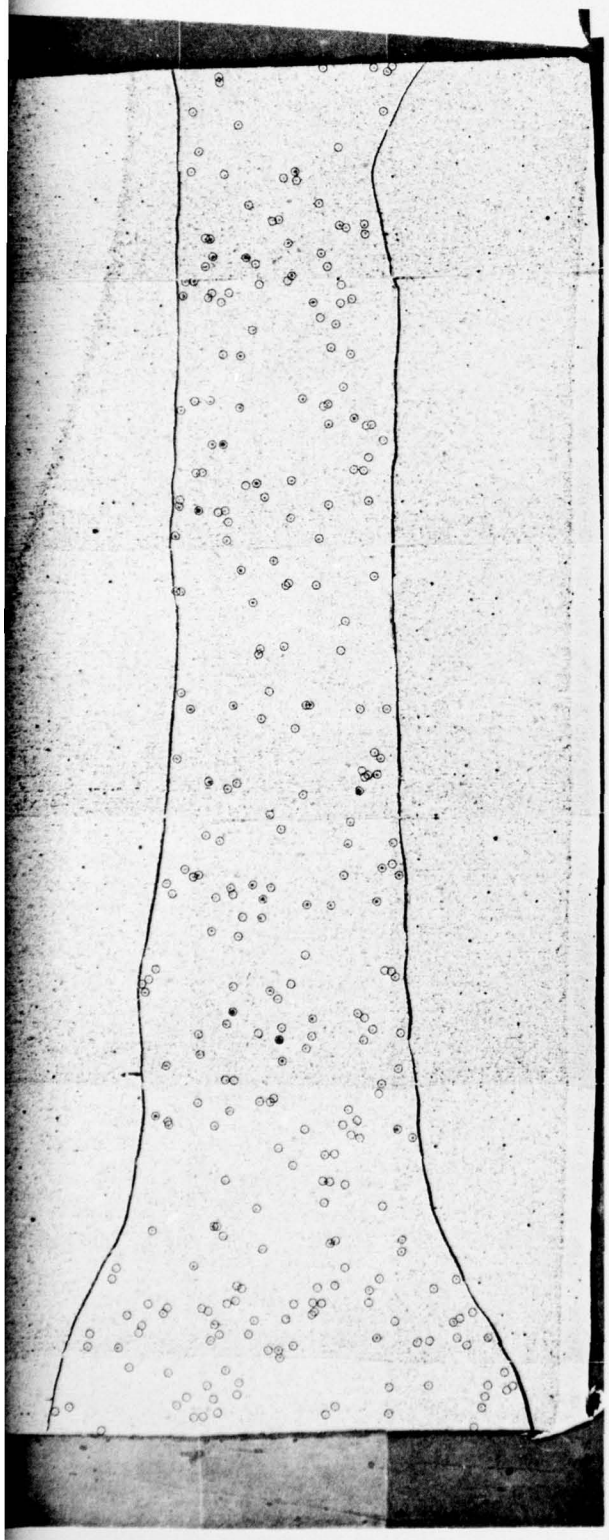

500 μ

R77–911989–10

DISTRIBUTION OF INCLUSIONS IN THE WELD FUSION ZONE AND EQUIVALENT ADJACENT AR

BASE METAL – 67 INCLUSIONS WELD FUSION ZON

(NOTE: REDUCTION IN MAGNIFICATION FROM ORIGINAL PHOTOGRAPHIC MAP REQU

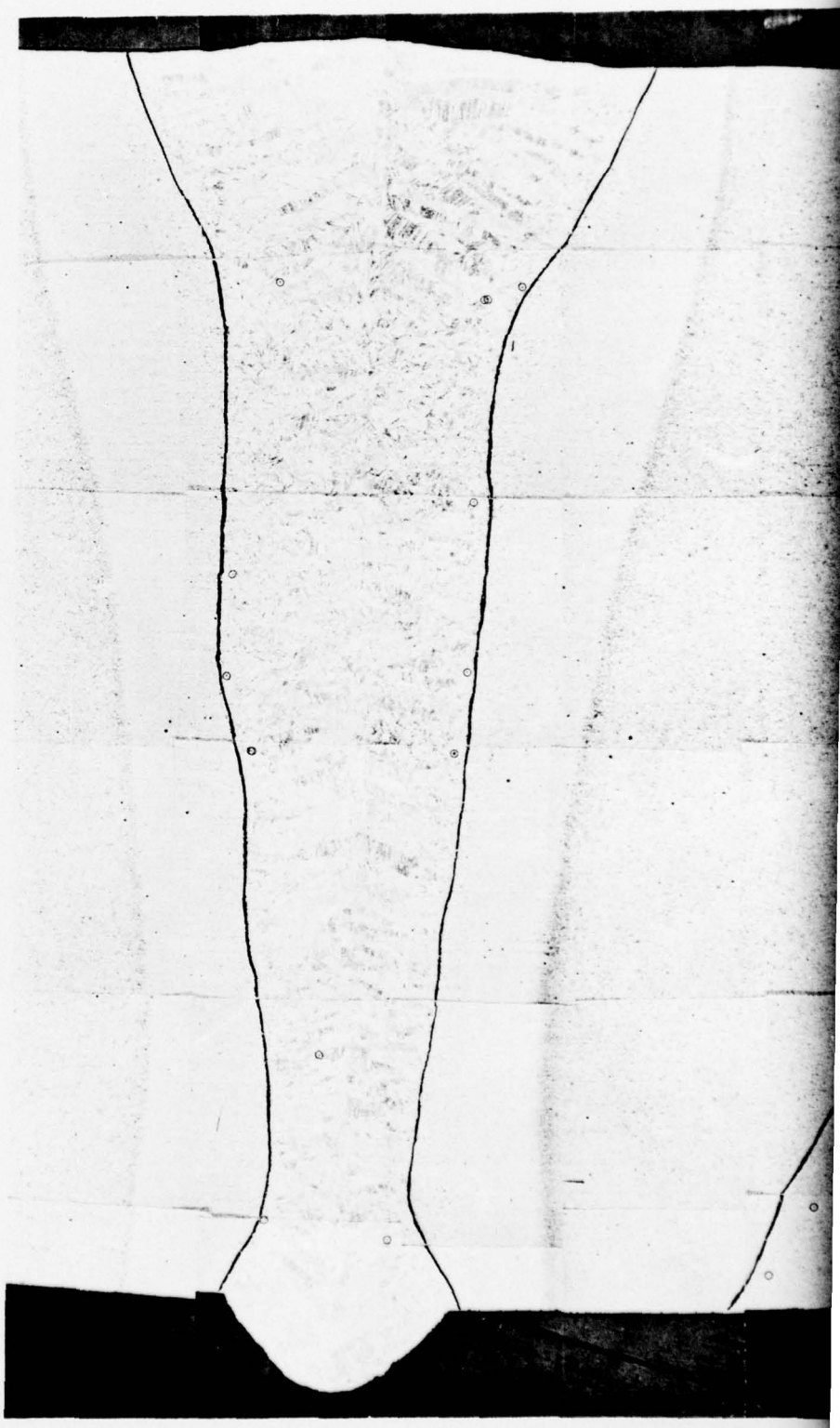

FIG. 19

IVALENT ADJACENT AREA OF BASE METAL IN HY–130 LASER WELD SPECIMEN C–7

NS WELD FUSION ZONE – 12 INCLUSIONS

NAL PHOTOGRAPHIC MAP REQUIRED ENCIRCLING OF INCLUSIONS FOR CLARITY.)

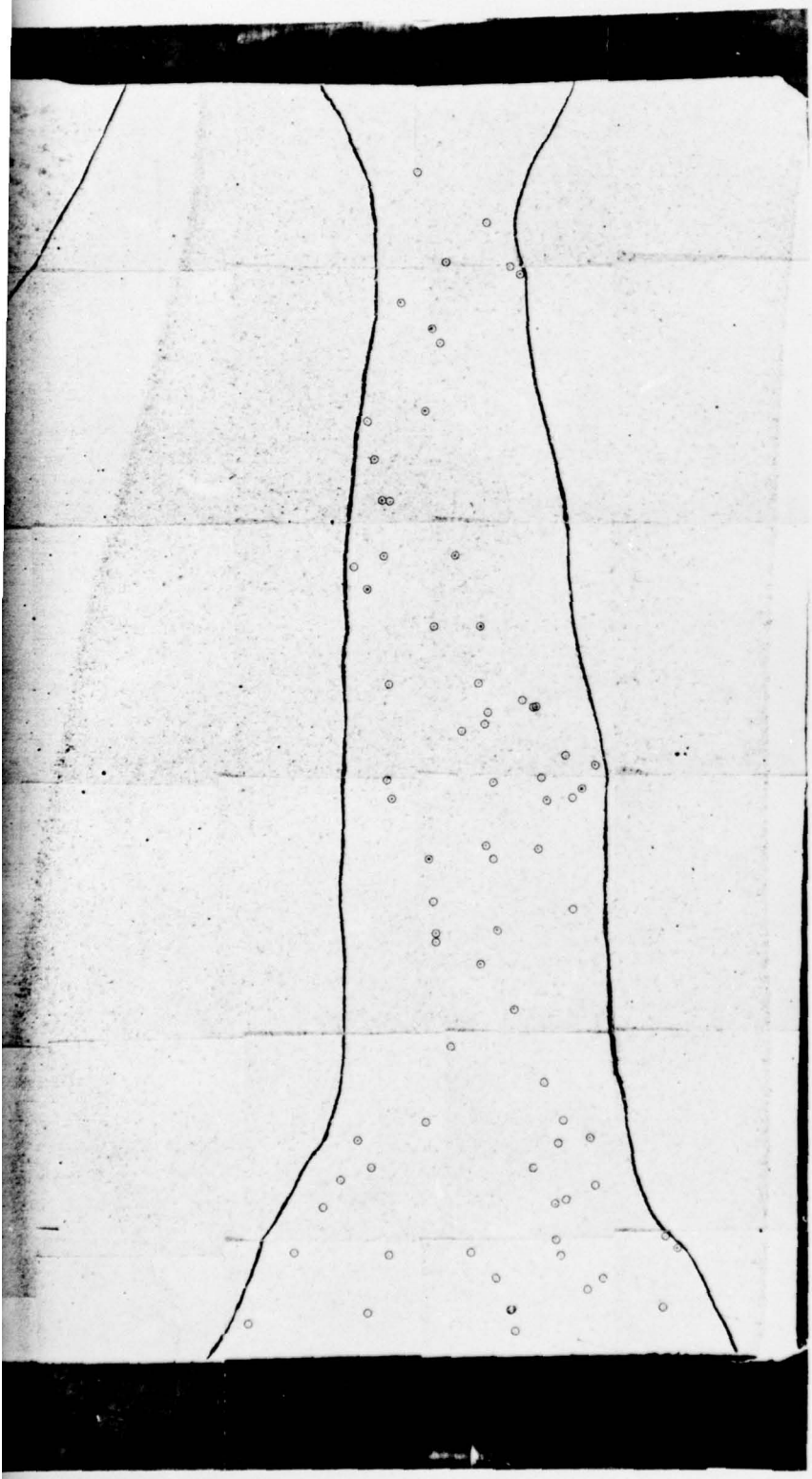

500 μ

FIG. 20

ELEMENTAL MICROPROBE ANALYSIS OF REPRESENTATIVE INCLUSION COMMON TO WELD AND BASE METAL OF 0.64 AND 0.95cm THICK HY-130 PLATE

ALUMINUM X-RAYS 2μ

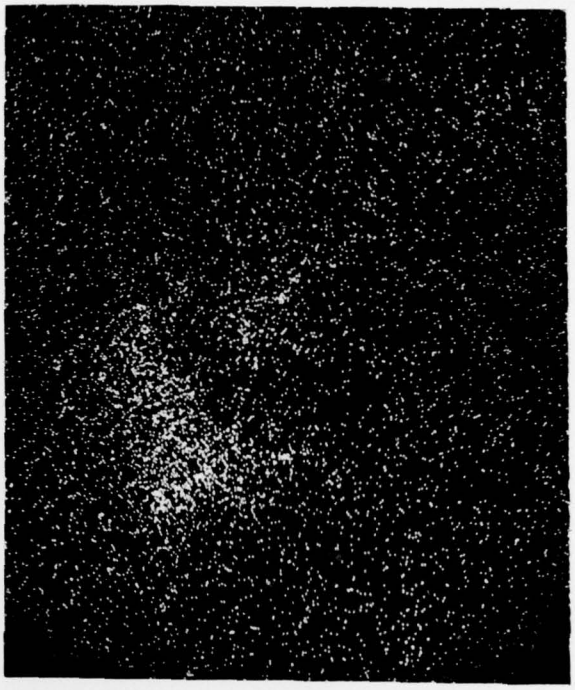

CALCIUM X-RAYS 2μ

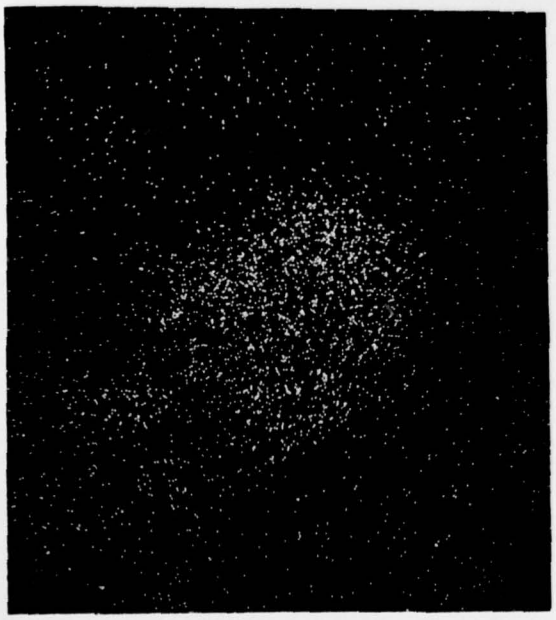

OXYGEN X-RAYS 2μ

BACKSCATTERED IMAGE 2μ

77-01-272-1

FIG. 21

ELEMENTAL MICROPROBE ANALYSIS OF REPRESENTATIVE INCLUSION COMMON TO WELD AND BASE METAL OF 1.27cm THICK HY–130 PLATE

(NOTE: ILLUMINESCENCE OF INCLUSION DURING ANALYSIS INDICATED INCLUSION WAS AN OXIDE)

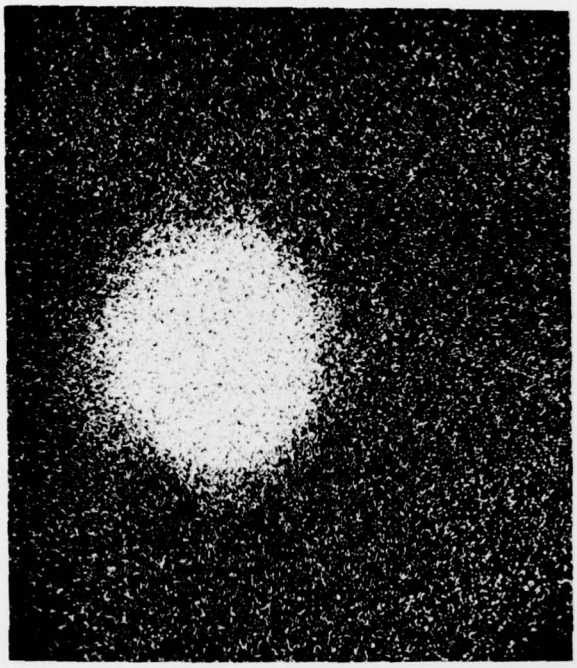

LANTHANUM X–RAYS 2μ

BACKSCATTERED IMAGE 2μ

(NOTE: DARK AREAS AROUND INCLUSION ARE VOIDS)

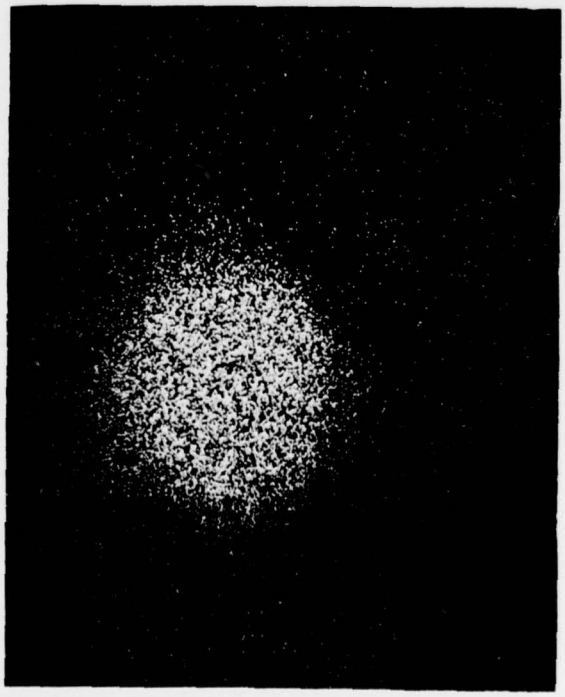

CERIUM X–RAYS 2μ

77–01–272–2